Brain, Behavior, and Immunity 97 (2021) 260–274

Contents lists available at ScienceDirect

Brain Behavior and Immunity

journal homepage: www.elsevier.com/locate/ybrbi

Gas6 drives Zika virus-induced neurological complications in humans and congenital syndrome in immunocompetent mice

Joao Luiz Silva-Filho [a,1], Lilian G. de Oliveira [b,1], Leticia Monteiro [a], Pierina L. Parise [c], Nagela G. Zanluqui [b], Carolina M. Polonio [b], Carla L. de Freitas [b], Daniel A. Toledo-Teixeira [c], William M. de Souza [d,e], Najara Bittencourt [a], Mariene R. Amorim [c], Julia Forato [c], Stéfanie P. Muraro [c], Gabriela F. de Souza [c], Matheus C. Martini [c], Karina Bispo-dos-Santos [c], Aline Vieira [c], Carla C. Judice [a], Glaucia M. Pastore [f], Eliana Amaral [g], Renato Passini Junior [g], Helaine M.B.P. Mayer-Milanez [g], Carolina C. Ribeiro-do-Valle [g], Roseli Calil [g], João Renato Bennini Junior [g], Giuliane J. Lajos [g], Albina Altemani [h], Marcos T. Nolasco da Silva [i], Ana Carolina Coan [j], Maria Francisca Colella-Santos [k], Andrea P.B. von Zuben [l], Marco Aurélio R. Vinolo [m], Clarice Weis Arns [m], Rodrigo Ramos Catharino [n], Maria Laura Costa [g], Rodrigo N. Angerami [l,o], André R.R. Freitas [l], Mariangela R. Resende [o], Márcia T. Garcia [o], Maria Luiza Moretti [o], Laurent Renia [p,q], Lisa F.P. Ng [p,q], Carla V. Rothlin [r], Fabio T.M. Costa [a,*], Jean Pierre Schatzmann Peron [b,s,t,*], José Luiz Proença-Modena [c,u,*]

[a] Laboratory of Tropical Diseases Prof. Luiz Jacintho Silva, Department of Genetics, Evolution, Microbiology and Immunology, Institute of Biology, University of Campinas, Campinas, Brazil
[b] Neuroimmune Interactions Laboratory, Department of Immunology, Institute of Biomedical Sciences, University of Sao Paulo, São Paulo, Brazil
[c] Laboratory of Emerging Viruses (LEVE), Department of Genetics, Evolution, Microbiology and Immunology, Institute of Biology, University of Campinas, Campinas, Brazil
[d] Virology Research Center, Ribeirão Preto Medical School, University of São Paulo, Ribeirão Preto, Brazil
[e] Department of Microbiology and Immunology, University of Texas Medical Branch, Galveston, TX, USA
[f] Faculty of Food Engineering, UNICAMP, Brazil
[g] Department of Obstetrics and Gynecology, School of Medical Sciences, University of Campinas, Campinas. Brazil
[h] Department of Clinical Pathology, School of Medical Sciences, University of Campinas, Campinas, Brazil
[i] Pediatric Immunology, Center for Investigation in Pediatrics, Faculty of Medical Sciences, UNICAMP, Brazil
[j] Department of Neurology, School of Medical Sciences, UNICAMP, Brazil
[k] Department of Human Development and Rehabilitation, School of Medical Sciences, UNICAMP, Brazil
[l] Campinas Department of Public Health Surveillance, Campinas, Brazil
[m] Department of Genetics, Microbiology and Immunology, Institute of Biology, UNICAMP, Brazil
[n] School of Pharmaceutical Sciences, UNICAMP, Campinas, Brazil
[o] Department of Internal Medicine, School of Medical Sciences, University of Campinas, Campinas, SP, Brazil
[p] A*STAR Infectious Diseases Labs (A* ID Labs), Agency for Science, Technology and Research, Biopolis, Singapore
[q] Singapore Immunology Network, Agency for Science, Technology and Research, Biopolis, Singapore
[r] Department of Immunobiology, Yale University, School of Medicine, New Haven, CT, United States
[s] Immunopathology and Allergy Post Graduate Program, School of Medicine, University of São Paulo, São Paulo, Brazil
[t] Scientific Platform Pasteur-USP, University of São Paulo (USP), São Paulo, SP, Brazil
[u] Experimental Medicine Research Cluster (EMRC), University of Campinas, Campinas, SP 13083-862, Brazil

ARTICLE INFO

Keywords:
Zika virus

ABSTRACT

Zika virus (ZIKV) has the ability to cross placental and brain barriers, causing congenital malformations in neonates and neurological disorders in adults. However, the pathogenic mechanisms of ZIKV-induced neurological

* Corresponding authors at: Department of Genetics, Evolution, Microbiology and Immunology, Institute of Biology, University of Campinas, Brazil (F.T.M. Costa, J.L. Proenca-Modena), Department of Immunology, Institute of Biomedical Sciences, University of Sao Paulo, Brazil (J.P. Schatzmann Peron).
E-mail addresses: costaftm@unicamp.br (F.T.M. Costa), jeanpierre@usp.br (J.P.S. Peron), jlmodena@unicamp.br (J.L. Proença-Modena).
[1] These authors equally contributed to this work.

https://doi.org/10.1016/j.bbi.2021.08.008
Received 17 June 2021; Received in revised form 2 August 2021; Accepted 5 August 2021
Available online 11 August 2021

TAM receptors
Type I Interferon
Socs1
Congenital infection

complications in adults and congenital malformations are still not fully understood. Gas6 is a soluble TAM receptor ligand able to promote flavivirus internalization and downregulation of immune responses. Here we demonstrate that there is a correlation between ZIKV neurological complications with higher Gas6 levels and the downregulation of genes associated with anti-viral response, as type I IFN due to *Socs1* upregulation. Also, Gas6 gamma-carboxylation is essential for ZIKV invasion and replication in monocytes, the main source of this protein, which was inhibited by warfarin. Conversely, Gas6 facilitates ZIKV replication in adult immunocompetent mice and enabled susceptibility to transplacental infection. Our data indicate that ZIKV promotes the upregulation of its ligand Gas6, which contributes to viral infectivity and drives the development of severe adverse outcomes during ZIKV infection.

1. Introduction

In 2015, Zika virus (ZIKV) emerged as an important global health problem, starting in South America, and then spreading to more than 94 countries worldwide. First discovered in 1947 in Uganda, Africa, it has not been considered a threat to human health, until the outbreaks in Yap, Micronesia (2007) and French Polynesia (2013). Most individuals are asymptomatic or develop a benign febrile disease characterized by cutaneous rash and conjunctivitis. However, it was further shown that ZIKV can cross the placental barrier and reach foetal tissues causing the congenital ZIKV syndrome (CZS), that may range from foetal growth restriction and microcephaly to severe retinal damage and arthrogryposis (Ioos, et al., 2014; Lupton, 2016; Duffy, et al., 2009). This was unprecedented and demanded great efforts of the scientific community to understand the underlying mechanisms involved in host-virus interaction, mainly those related to susceptibility and pathogenicity.

Central nervous system (CNS) manifestations after congenital infection, such as brain calcifications, lissencephaly, ventriculomegaly and microcephaly, are among the most notable and concerning outcomes of ZIKV infection in newborns (Mlakar, et al., 2016; França, et al., 1501; , Ventura 2016). However, severe ZIKV infection is not limited to newborns: neurological manifestations as acute myelitis, encephalitis, meningoencephalitis and Guillain-Barré syndrome can also occur in adults (Cao-Lormeau, et al., 2016; Waggoner, 2016; Kam et al., 2017). This raises not only the question on what are the genes that confer susceptibility to ZIKV neuropathology, but also, what are the cellular and molecular mechanisms orchestrating such phenomenon. In this context, we believe the interaction between viral particles with host cells, the first step of infection, may be of pivotal relevance. This interaction dictates more than the viral tissue tropism, but also triggers a diversity of intracellular pathways that may greatly account for either failure or success of infection (Moller-Tank and Maury, 2014; Laureti, et al., 2018).

Growth arrest-specific 6 (Gas6) is a 75 KDa secreted protein composed of an N-terminal Gla domain, followed by four epidermal growth factor (EGF)-like domains and a C-terminal SHBG domain (van der Meer and van der Poll, 2014). Upon γ-carboxylation of the Gla domain, Gas6 is able to interact with TAM (Tyro3, Axl and Mer) receptors and phosphatidylserine (PtdSer) promoting phagocytic internalization of the apoptotic bodies (van der Meer and van der Poll, 2014). TAM activation triggers different signalling pathways involved in cell survival, mainly orchestrated by PI3K and Akt (van der Meer and van der Poll, 2014; Lemke and Rothlin, 2008). Interestingly, PtdSer containing viruses, such as flaviviruses and filoviruses, may also bind to Gas6, activating clathrin-mediated phagocytic internalization and subverting cellular immune response by activating negative regulators of anti-viral cytokines, as SOCS-1 and SOCS-3 (Moller-Tank and Maury, 2014; Laureti, et al., 2018; Rothlin et al., ,2007), negatively regulating type I interferon receptor (IFNAR) signalling pathway (van der Meer and van der Poll, 2014; Lemke and Rothlin, 2008; Rothlin et al., 2007; Chen 2018; Meertens et al., 2017; Hamel et al., 2015; Hastings et al., 2019). However, the overall interplay of viral and host factors, such as Gas6, that orchestrate the clinical course of ZIKV infection is not fully understood.

Here we investigated the role of Gas6 in the pathogenesis of ZIKV infection both in human samples and murine model. We observed that circulating levels of Gas6 are upregulated in the serum of ZIKV-infected patients, including pregnant women, and a further increase occurs in patients with neurological complications. Concurrently, there is a reduced transcriptional expression of genes associated with type I IFN responses and other immune signatures, as consequence of *Socs1* upregulation in peripheral blood cells. ZIKV infected monocytes were an important source of Gas6 production, and Gas6 gamma-carboxylation was essential for ZIKV cellular invasion and replication. Conversely, we also demonstrated that Gas6 is upregulated in ZIKV-infected pregnant mice and that pre-incubation of ZIKV with recombinant Gas6 facilitates ZIKV replication and rendered them susceptible to transplacental infection and modulating placental Type I IFN. We thus propose that Gas6 not only favours viral invasion and replication, but also dampens antiviral immune responses. Collectively, our data brings novelty to the role of Gas6 on the understanding of ZIKV pathogenesis as a relevant host factor driving severe outcomes, such as neurological complications and vertical transmission. Addressing this issue could help develop predictive approaches for early diagnostics and open new possibilities to develop effective treatment against severe complications.

2. Results

2.1. Gas6-producing monocytes dampen the antiviral response during ZIKV infection

Monocytes are the dominant cell type infected by ZIKV among peripheral blood cells (Foo, et al., 2017; Michlmayr, et al., 2017). To further understand the role of Gas6 in facilitating ZIKV replication, we used both cultured human monocytes (THP-1 cells) and PBMCs from healthy donors infected with ZIKV (Brazilian strain BeH823339) at MOI 0.1, 1 and 10. We sought to investigate whether ZIKV infection may induce increased Gas6 secretion. Cell pellets and their respective supernatants were collected at different time points post-infection, and Gas6 levels were determined by qRT-PCR and ELISA, respectively. Both THP-1 (Fig. 1A-B) and PBMCs (Fig. 1D-E) had increased Gas6 secretion after ZIKV infection with time, especially at higher MOIs. Conversely, there was a direct correlation of Gas6 secretion and ZIKV replication (Fig. 1C, F).

To determine whether increased Gas6 production correlates with transcriptional changes induced by infection we verified the gene expression profile of these cells. As γ -glutamyl carboxylation of Gas6 via vitamin-K-dependent enzyme γ-glutamyl carboxylase (GGCX) and Vitamin-K epoxide reductase enzyme complex 1 (VKORC1) (Davra et al., 2016) is needed for Gas6 biological activity and to bridge enveloped viruses to TAM receptors (Davra et al., 2016; Meertens, et al., 2012; Bhattacharyya, et al., 2013; Perera-Lecoin, et al., 2013; Nakano, et al., 1997), we checked the expression of these related molecules. Interestingly, as shown in Fig. 1G, the heatmap shows that Gas6 mRNA is upregulated in THP-1 cells as soon as 6 h p.i. and remains increased throughout the experiment (Fig. 1G and Supp Fig. 1B). GGCX and VKORC1 mRNA expression were not significantly altered, although it tends to decrease at higher MOI 10 (Fig. 1G, Supp Fig. 1B). In agreement

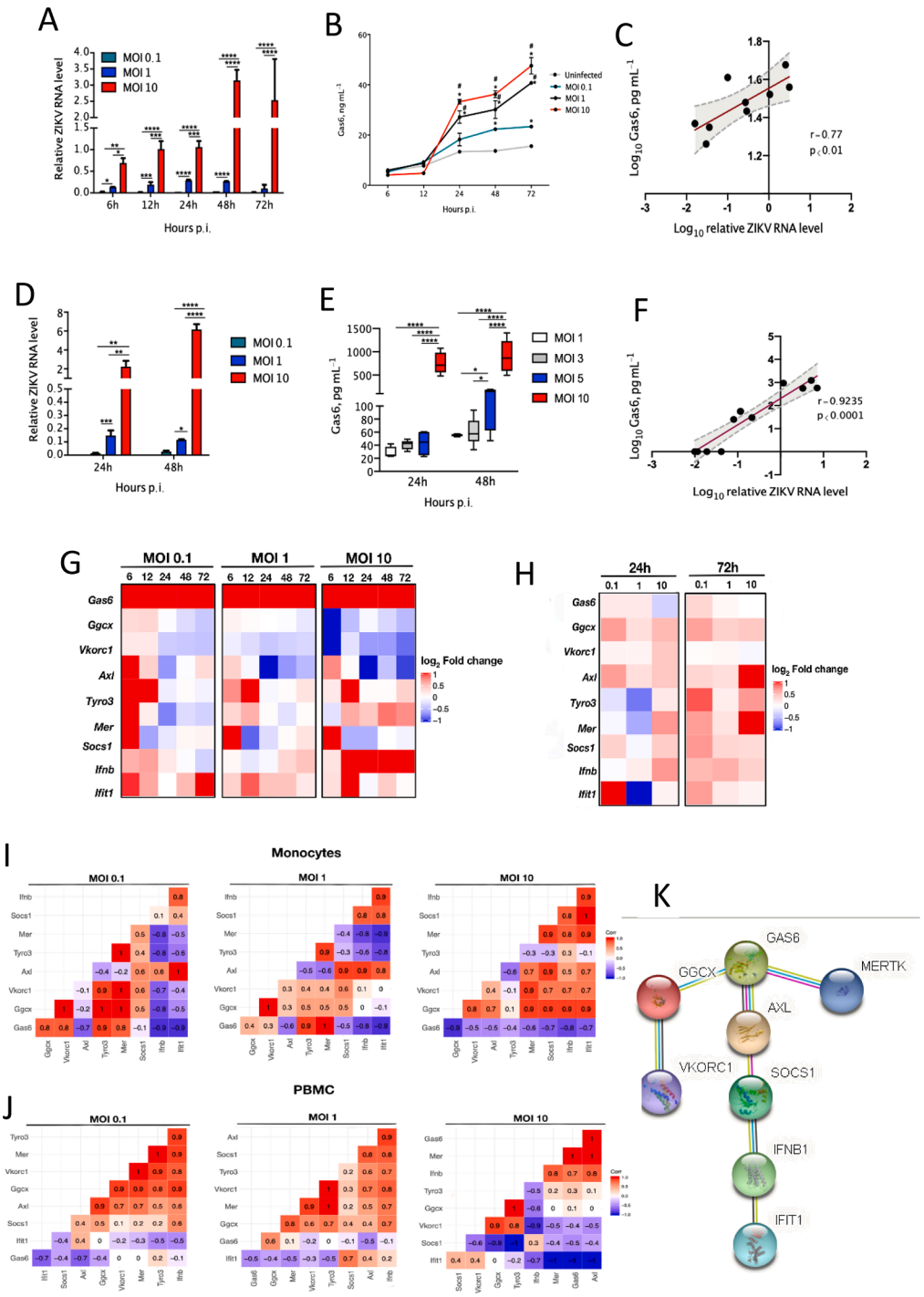

Fig. 1. ZIKV infection stimulates Gas6 upregulation and leads to downregulation of type I IFN response in THP-1 cell line an peripheral blood mononuclear cells (PBMCs). PBMCs and THP-1 monocytes were challenged with ZIKV (MOI 0.1, 1 and 10), respectively (A, D). Gas6 levels were determined by ELISA in the supernatant of THP-1 cells (B) and PBMCs (C) from healthy donors collected after *in vitro* infection with ZIKV at different multiplicities of infections (MOI 0.1, 1 and 10). Significance was calculated for comparisons between MOIs at the corresponding time point using Kruskal-Wallis test with post hoc correction for multiple testing using the original FDR method of Benjamini and Hochberg were conducted. *$p < 0$ 0.05; **$p < 0.01$; ***$p < 0$ 0.001, ****$p < 0.0001$. Correlation plots comparing logarithmically transformed ZIKV RNA levels with Gas6 concentration within matched cell and supernatant from THP-1 monocytes (C) or PBMCs (F). Regression line indicated in red with 95% confidence area shown in shaded gray. Pearson's (C) Spearman's Rank (F) correlation coefficient and associated p-values are shown. Total cellular RNA from both THP-1 (G) and PBMCs (H) was extracted at different time points after infection as indicated in the graphs, and relative *GAS6*, *GGCX*, *VKORC*, *AXL*, *TYRO3*, *MER*, *SOCS1*, *IFNb1* and *IFIT1* mRNA levels were determined by real-time quantitative PCR. The data shown are mean ± SEM representative of two independent experiments using cells from different donors. Significance was calculated for comparisons between conditions at the corresponding time point using One-way analyses of variance statistical test with Bonferroni-corrected multiple comparisons test. *$p < 0$ 0.05; **$p < 0.01$; ***$p < 0$ 0.001, ****$p < 0.0001$. The data shown are representative images of three independent experiments. Representative images of the Spearman's Rank Correlations matrix (I, J). Correlations were determined to assess the association between transcripts quantified in the THP-1 monocytes (I) or PBMCs (J), after *in vitro* infection with ZIKV at different multiplicities of infections (MOI 0.1, 1 and 10). Correlation network obtained from STRING database with the input of target proteins (K). (For interpretation of the references to colour in this figure legend, the reader is referred to the web version of this article.)

with a previous study (Sun, et al., 2017), Axl, Mer, Tyro3 and SOCS-1 mRNA expression was increased early after infection (6–12 h p.i.) mainly at lower MOI 0.1and early timepoints (Fig. 1G, Supp Fig. 1B). IFN-β is upregulated only at MOI 10 (Fig. 1G, Supp Fig. 1B), but the cells are irresponsive, as IFIT-1expression does not significantly change in comparison to uninfected cells (Fig. 1G). A late significant increase (72 h p.i.) of IFIT-1 mRNA expression is observed only at the lower MOI 0.1 (Fig. 1G, Supp Fig. 1B).

In PBMCs cells, a slight upregulation of GGCX mRNA expression is observed 24 h and 72 h p.i in infected cells at all MOIs, while VKORC1 mRNA expression was not affected (Fig. 1H, Supp Fig. 1A). Importantly, ZIKV infection induces upregulation of Axl, Tyro and Mer transcripts at higher MOI 10 mainly at 72 h p.i. (Fig. 1H, Supp Fig. 1A). SOCS-1 is upregulated in ZIKV-infected PBMCs at all MOIs (Fig. 1H, Supp Fig. 1A), except for MOI 1 at 24 h. Interestingly, although IFN-β mRNA is upregulated later during infection (72 h p.i.), the cells seem irresponsive, as IFIT-1 mRNA expression does not change in comparison to uninfected cells at MOIs 1 and 10 (Fig. 1H, Supp Fig. 1A). Only at the lower viral load (MOI 0.1) at 24 h p.i. a significant upregulation of IFIT-1 mRNA expression is observed (Fig. 1H, Supp Fig. 1A), which later decreases at 72 h. Interestingly, in PBMCs, Gas6 expression negatively correlates with IFIT-1 at all viral loads (Fig. 1J) while in THP-1 cells, Gas6 negatively correlates with IFN-β and IFIT-1 at all viral loads (Fig. 1I). Altogether, these data show that ZIKV infection induces a significant upregulation of Gas6 production in monocytes, which in turn facilitates viral replication by suppressing type I IFN antiviral response. The correlation of Gas6 with type I IFN response is corroborated by Gas6 network interactions at STRING (Fig. 1K).

2.2. Inhibition of Gas6 γ-glutamic acid carboxylation (Gla domain) restores antiviral response

To further determine the mechanistic link between Gas6 production, ZIKV replication and suppression of antiviral response, we tested whether inhibiting Vitamin-K-dependent γ-carboxylation of Gas6 glutamic acid residues (Gla domain) restores antiviral immune response and controls viral replication. For that we used low-dose warfarin, which specifically block γ-carboxylation of Gla domain in Gas6, resulting in decreased TAM receptor activation (Davra et al., 2016; Nakano, et al., 1997; Kirane, et al., 2015). In parallel, we used R428, a well-known inhibitor of Axl tyrosine kinase activity tested in ZIKV infection (Meertens, et al., 2017). THP-1 cells were infected with ZIKV at MOI 1 and treated with 2 μM of warfarin or 2 μM R428 throughout the course of infection (up to 72 h). Treatments started at the moment of infection or 2 h.p.i. (after virus entry), and cell pellets and their respective supernatants were collected at different time points. Both warfarin and R428 treatment significantly reduced Gas6 secretion (Fig. 2A), while mRNA levels were decreased only during warfarin treatment (Fig. 2D). Warfarin completely abrogated the production of ZIKV infectious particles at 72 h p.i (Fig. 2B) while R428 showed a modest but significant effect on decreasing viral production at 72 h p.i (Fig. 2C). Unexpectedly, ZIKV RNA level did not change in both treatments (Supp. Fig. 2A, B).

Accordingly, inhibition of Gla-domain γ-carboxylation by warfarin restored *IFNβ* and *IFIT-1* expression and reduced Gas6 secretion, consistent with the reduction in GCKX and VKOC expression (Fig. 2C). Corroborating this, R428 increased the expression of *AXL* and *MER* and restored *IFN-β* and *IFIT-1* expression, whereas *GGCX* and *VKORC1* mRNA expression were not affected (Fig. 2D). Finally, the flow cytometry analysis indicated that the percentage of ZIKV NS1 positive-cells were decreased when Vero cells were cocultured with supernatants from warfarin-treated THP-1 cells, regardless of whether the initial virus inoculum was washed-out 2 h p.i. or not, or whether warfarin treatment started at the moment of infection or 2 h p.i. (Supp Fig. 3). Thus, blockage of Gas6 activity by inhibition of γ-carboxylation of Gla domain or tyrosine kinase signalling restores type I IFN antiviral response reducing viral replication. Collectively, these data show the mechanism by which Gas6 upregulation contributes to a higher ZIKV infection.

2.3. Increased Gas6 expression in ZIKV adult patients with neurological complications

To correlate Gas6 levels to the pathogenesis of ZIKV-associated neurological complications, we determined Gas6 levels by ELISA in serum from patients, included in a cross-sectional study realized between February 2016 and June 2017 in different hospitals in the city of Campinas, Brazil (Kam et al., 2017). In this study was included samples from 57 patients with a mild disease by ZIKV (Non-Neuro^{ZIKV}), 19 from patients with neurological complications after ZIKV infection (Neuro^{ZIKV}), 14 from patients with neurological complications but with no indicia of ZIKV infection (Neuro$^{NON\text{-}ZIKV}$) and 13 from healthy donors (HD). Table 1 summarizes the demographic data and clinical manifestations of the patients included in this study.

Interestingly, circulating levels of Gas6 were significantly increased in ZIKV-infected patients compared to healthy donors (Non-Neuro^{ZIKV}: 22.56 ng/mL [25–75 interquartile range (IQ) 14.6–29.9] versus 13.36 ng/mL [25–75 IQ 11.6–16.1] in HDs, $p = 0.0062$) (Fig. 3A), whose circulating Gas6 levels were comparable to previous studies (Papa, et al., 2017; Morizono, et al., 2011; Ozakpinar, et al., 2016). Importantly, Neuro^{ZIKV} patients showed a further increase of serum Gas6 in comparison to Non-Neuro^{ZIKV} patients (33.05 ng/mL [25-75IQ 22.5–40.2], $p = 0.0289$) (Fig. 3A). To rule out the possibility of co-infections influencing Gas6 levels observed in these patients, we used a high-throughput screening (HTS) virus metagenomic approach to identify viral co-infections that were not detected by RT-qPCR or diagnosed by laboratory tests. ZIKV mono-infections in the Neuro^{ZIKV} patients were confirmed in 9 out of 10 patients tested. In one patient, the complete genome of a strain of Pegivirus C (*Pegivirus* genus, *Flaviviridae* family) was sequenced (Supp Fig. 4). Noteworthy, this virus has not been associated with neurological complications in humans. Finally, unchanged Gas6 levels in the serum of 14 patients with neurological diseases non-related to acute ZIKV infection (Neuro$^{NON\text{-}ZIKV}$) revealed that Gas6 upregulation is a ZIKV-specific response (Fig. 3A). Genotyping analysis revealed no difference in *GAS6* haplotypes between the ZIKV-infected patient groups, both showing a predominant frequency of the c.834 + 7G > A AA genotype (Fig. 3B).

2.4. Gas6 upregulation suppresses antiviral IFN response in ZIKV adult patients with neurological complications

To determine the mechanisms by which ZIKV-induced Gas6 upregulation contributes to the pathogenesis of neurological complications in adult patients, we used network analysis of biomarkers and transcriptional profiling to determine how Gas6 orchestrates with a specific signature of immune mediators associated with ZIKV infection, previously determined in our cohort (Kam et al., 2017). In accordance with its role as pleiotropic inhibitor of innate immune responses (van der Meer and van der Poll, 2014; Lemke and Rothlin, 2008; Meertens, et al., 2017), Gas6 negatively correlated with several pro-inflammatory cytokines/chemokines, such as IL-2, IL-8, IL-27, RANTES, IP-10 and TNF-α (r greater than 0.7; $p < 0.05$) in healthy donors (Supp. Fig. 5A, B). Interestingly, a striking change in the pattern of interactions between all biomarkers appeared in Non-Neuro^{ZIKV} patients (Supp. Fig. 5C, D). In these patients, Gas6 significantly and positively correlates only with IFN-α ($r = 0.60$; $p < 0.05$), apart from other 2 functional clusters of significant interactions between the measured biomarkers (Supp. Fig. 5C, D). In addition, the network graph of Non-Neuro^{ZIKV} patients is more heterogeneous and shows a decentralized topology with lower complexity and connectivity between the immune mediators when compared to the highly dense, homogenous and centralized graph of HDs (Non-Neuro^{ZIKV} vs HDs network density: 0.120 vs 0.224; network centralization: 0.107 vs 0.335; network diameter: 10 vs 5) (Supp. Fig 6B, D). Interestingly, a further increase on Gas6 levels above certain

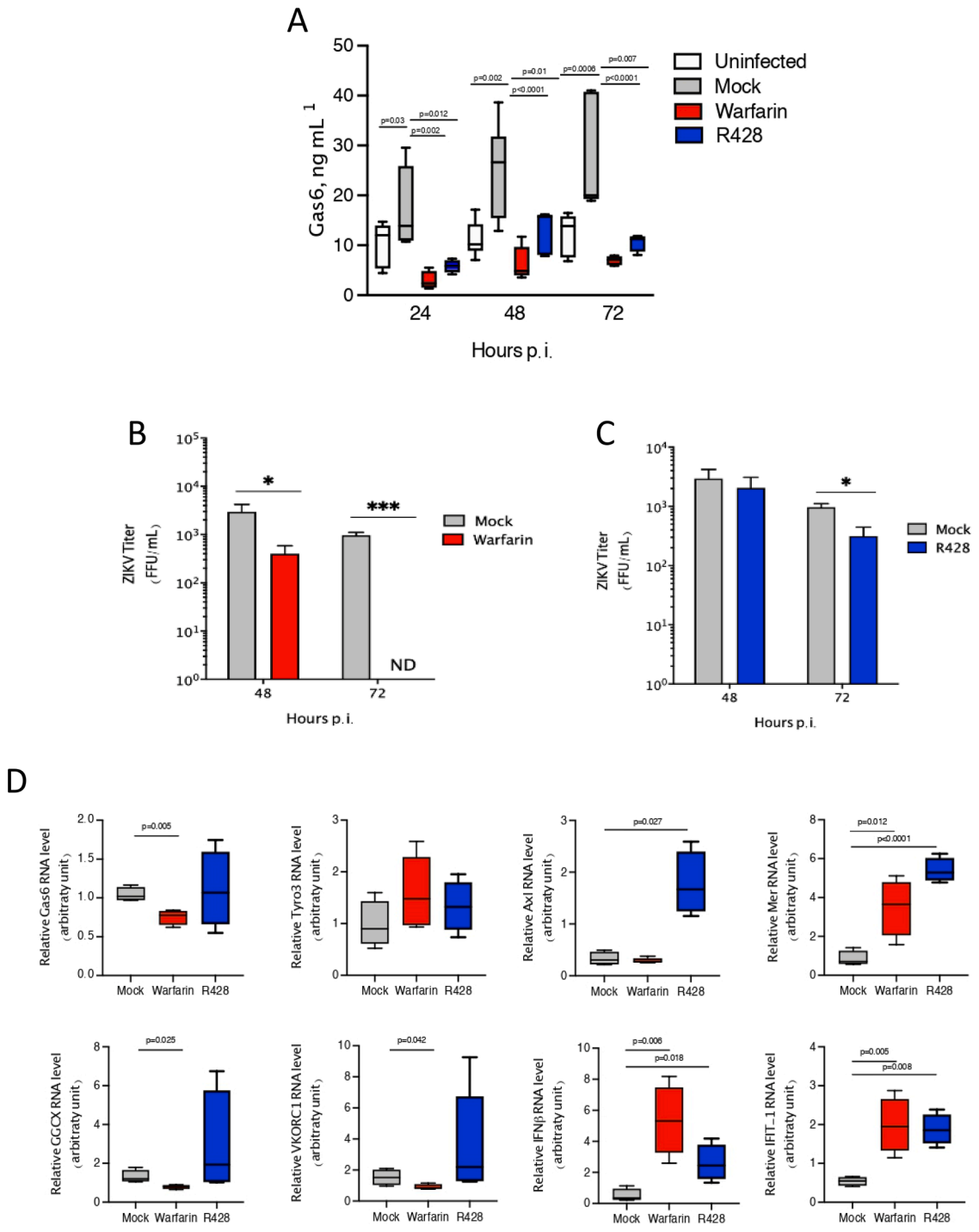

Fig. 2. Inhibition of Gas6 γ-glutamic acid carboxylation (Gla domain) by warfarin and blockage of AXL tyrosine kinase domain by R428 treatment restores antiviral response. Gas6 levels were determined by ELISA in the supernatant of THP-1 monocytes collected at 24 h, 48 h and 72 h after *in vitro* infection with ZIKV (MOI 1). Infected cells were treated or not (mock) with 2 μM warfarin or R428 throughout the course of infection. Gas6 concentration is depicted as Tukey box plots (A). The data shown are representative images of three independent experiments. Significance was calculated for comparisons between conditions at the corresponding time point using One-way analyses of variance statistical test with Bonferroni-corrected multiple comparisons test. *$p < 0$ 0.05; **$p < 0.01$; ***$p <$ 0 0.001, ****$p < 0.0001$. ZIKV titer (FFU/mL) was determined by focus-forming assay after incubation of ZIKV-permissive Vero E6 cell line with the 48 h or 72 h supernatant from THP-1 cells (B and C). Total cellular RNA was extracted at different time points after infection. Relative viral RNA levels, *GAS6*, *GGCX*, *VKORC*, *AXL*, *TYRO3*, *MER*, *SOCS1*, *IFNb1* and *IFIT1* mRNA levels were determined by real-time quantitative PCR after infection and treatment with warfarin and R428 (D). The data shown are representative images of three independent experiments. Graphs depict relative RNA expression as Tukey box plots after results were normalized to *GAPDH* housekeeping gene expression. A student's *t*-test was used to compare groups with normally distributed data, and a Mann-Whitney test was used to compare groups with non-normal distributions; *$p < 0.05$; **$p < 0.01$; ***$p < 0.001$; ****$p < 0.0001$. The data shown are representative images of three independent experiments. A Mann-Whitney test was used to compare conditions at the corresponding time point. *$p < 0.05$; **$p < 0.01$; ***$p < 0.001$; ****$p < 0.0001$.

Table 1
Sociodemographic, clinical and laboratorial findings in the considered groups included in this study.

Characteristic	Patients No (%)			
	Non-Neuro^{ZIKV}(n = 57)	Neuro^{ZIKV}(n = 19)	Neuro$^{NON-ZIKV}$(n = 14)	HD(n = 13)
Demographics				
Age, median (range) in years	31 (1–69)	32 (1–82)	26 (1–74)	29 (18–45)
Female sex	42 (73.7)	11 (57.8)	6 (42.8)	8 (61.5)
Preceding symptoms				
Fever	35 (61.5)	10 (52.6)	7 (50.0)	NA
Rash	37 (65)	8 (42.1)	4 (28.5)	NA
Conjunctivitis	24 (42.1)	7 (36.8)	2 (14.3)	NA
Headache	22 (38.6%)	5 (26.3)	3 (21.4)	NA
Arthralgias	12 (21%)	3 (15.7)	3 (21.4)	NA
Myalgias	19 (33.3%)	2 (10.5)	1 (7.2)	NA
Time from onset of viral symptoms to ZIKV diagnosis, median (range) in days	3 (0 – 10)	4 (1 – 10)	NA	NA
Laboratory tests				
ZIKV viral load in urine (median of copies/mL)	2079	2049	NA	NA
NS1/IgM DENV detection	0 (0.0)	0 (0.0)	3 (21.4)	0 (0.0)
DENV qRT-PCR	0 (0.0)	0 (0.0)	0 (0.0)	0 (0.0)
CHIKV qRT-PCR	0 (0.0)	0 (0.0)	0 (0.0)	0 (0.0)
OROV qRT-PCR	0 (0.0)	0 (0.0)	0 (0.0)	0 (0.0)
Neurological diagnosis				
Guillain-Barré syndrome	NA	5 (26.3)	3 (21.4)	NA
Encephalitis	NA	6 (26.3)	7 (50)	NA
Meningitis	NA	4 (31.6)	2 (14.2)	NA
Meningoencephalitis	NA	3 (15.8)	2 (14.2)	NA
Transverse myelitis	NA	1 (2.6)	0 (0)	NA
Time from onset of viral symptoms to neurological symptoms, median (range) in days	NA	4 (2 – 15)	7 (1–29)	

Samples of 8 ZIKV-infected pregnant women and 6 infants born of these women were also analysed in this study. Two of these infants had growth restriction and CNS alterations compatible with CZS. Due the small number of patients, no clinical comparison was made between these two groups.

threshold (estimated to be above 30 ng/mL), as observed in Neuro^{ZIKV} patients (Fig. 3C, D), greatly changes the patterns of interactions (Supp. Fig. 5E, F). In these patients, Gas6 displays positive correlation with IL-1RA, IL-6, MCP-1 and IP-10 ($r = 0.8$; 0.5, 0.4 and 0.3, respectively; $p < 0.05$) and negative correlations with IFN-α, IFN-γ and IL-18 ($r = -0.4$; −0.7 and −0.5, respectively; $p < 0.05$) (Fig. 3C, D). In addition, as shown in the network graph (Fig. 3D), because IFN-γ forms a functional cluster of interactions with a variety of cytokines with key roles in the antiviral response, Gas6 also displays indirect negative correlations with TNF-α, IL-1β, IL-12, IL-22 and IL-27 (r between −0.3 and −0.5; $p < 0.05$), as shown in Fig. 3C.

To confirm whether Gas6 drives suppression of antiviral response, we conducted quantitative mRNA expression analysis in peripheral blood cells isolated from healthy donors and patients with and without neurological complications. Expression of Axl and Mer is upregulated in the peripheral blood cells from Neuro^{ZIKV} patients (Fig. 3F, G), whereas Tyro3 did not change (Fig. 3E). In accordance with TAM-induced SOCS upregulation (Lemke and Rothlin, 2008; Alciato, et al., 2010), we observed a significant increase of SOCS1 mRNA in circulating cells from Neuro^{ZIKV} patients (Fig. 3H). Conversely, mRNA expression of IFN-β and IFIT-1 is significantly reduced (Fig. 3I, J). Thus, in ZIKV adult patients, increased circulating Gas6 levels has a negative correlation with *Ifnb* and *Ifit1* gene expression and positively correlates with *Axl* and *Socs1* expression in peripheral blood cells (Fig. 3K).

Also, it is interesting to mention that Gas6 negatively correlated with FGF-2 in Neuro^{ZIKV} patients (Fig. 3C-D). This led us to think that Gas6 may also correlate with fibroblasts function and extracellular collagen and fibronectin production. This was confirmed by STRING database network analysis of Gas6, showing that Gas6 interacts with FN1 and several types of collagens as COL1A1, COL1A2 (Fig. 3L). Interestingly, fibronectin and collagen has already been described to be important for ZIKV-associated microcephaly development, which indicated that Gas6 may not only correlated with suppression of the immune response, but also to disruption of blood brain barrier (BBB). In this sense, we also evaluated the correlation between ZIKV, Gas6 and endothelial cells by using human brain microvascular endothelial cells (hBMECs). As shown in Supp Fig 6A and B, ZIKV infection does not stimulate Gas6 production by hBMECs, indicating that blood mononuclear cells might be the main source of circulating Gas6 during ZIKV infection as demonstrated in Fig. 3A and B. However, this does not exclude the possibility that Gas6 may favour BBB disruption.

2.5. Gas6 facilitates ZIKV replication in immunocompetent mice

So far, our data show that Gas6 expression is stimulated during ZIKV infection, and it is associated with neurological complications in human patients. The underlying pathogenic mechanism of Gas6 involves attachment and invasion and facilitation of viral replication by suppressing the antiviral response. Although we showed a correlation between Gas6 levels, ZIKV RNA load and production of infecting particles in infected cells *in vitro*, we could not find the same association in our cross-sectional cohort. To confirm that upregulation of Gas6 favours viral replication *in vivo*, immunocompetent adult C57BL/6 and SJL mice were intravenously infected with 10^2 pfu ZIKV (BeH815744) previously incubated or not with 1 μg/mL recombinant mouse Gas6 (ZIKV^{rmGas6}) (Fig. 4A). Viral load was determined at 1, 3 and 5 d.p.i. in the spleen and serum. Interestingly, infection with Gas6-coated ZIKV resulted in increased viral RNA in the spleen (Fig. 4B, C) in both strains at 1 d.p.i. After 3 and 5 days of infection, differences were no longer detected. Similar to *in vitro* infection of cultured human cells, these data corroborate the role of Gas6 in favouring ZIKV infection and replication.

2.6. Gas6 promotes transplacental infection in ZIKV-infected immunocompetent mice

To further evaluate whether Gas6 correlates with disease severity during ZIKV infection, we evaluated its association with transplacental infection and foetal pathology. Determination of Gas6 levels in the serum of 8 ZIKV-infected pregnant women revealed a significant increase during acute phase of infection (18.05 ± 1.97 ng/mL versus 13.36 ± 1.23 ng/mL) (Supp Fig. 7A). On the other hand, we did not detect a difference in Gas6 levels in the serum of the babies with ($n = 2$) or without ($n = 4$) CZS (Supp Fig. 7B).

As the number of ZIKV-infected pregnant women with foetal growth-associated malformations included in this study was limited to two patients, we decided to evaluate the effect of Gas6 using a mouse model of CZS. For this, we subcutaneously injected pregnant C57BL/6 mice with Gas6-coated ZIKV (ZIKV^{rmGas6}) at embryonic day (E) 16 and performed analysis at E18 or postnatal day (P) 4 (Fig. 4D). Importantly, infection of pregnant C57BL/6 mice with ZIKV^{rmGas6} rendered their offspring susceptible to foetal malformations. We evidenced macroscopic changes at E18 (Fig. 4E) and growth delay at P4 (Fig. 4F). Significant differences in crown-rump, skull length and weight of the ZIKV^{rmGas6} newborns were observed in comparison with control group (Fig. 4F). Importantly, no differences were observed between ZIKV and control group. Surprisingly, no difference in the viral load between ZIKV and ZIKV^{rmGas6} groups was found in the placenta and foetal spleen at E18 (Supp Fig. 8C) as well as in the spleen of P4 newborns (Supp Fig. 8E).

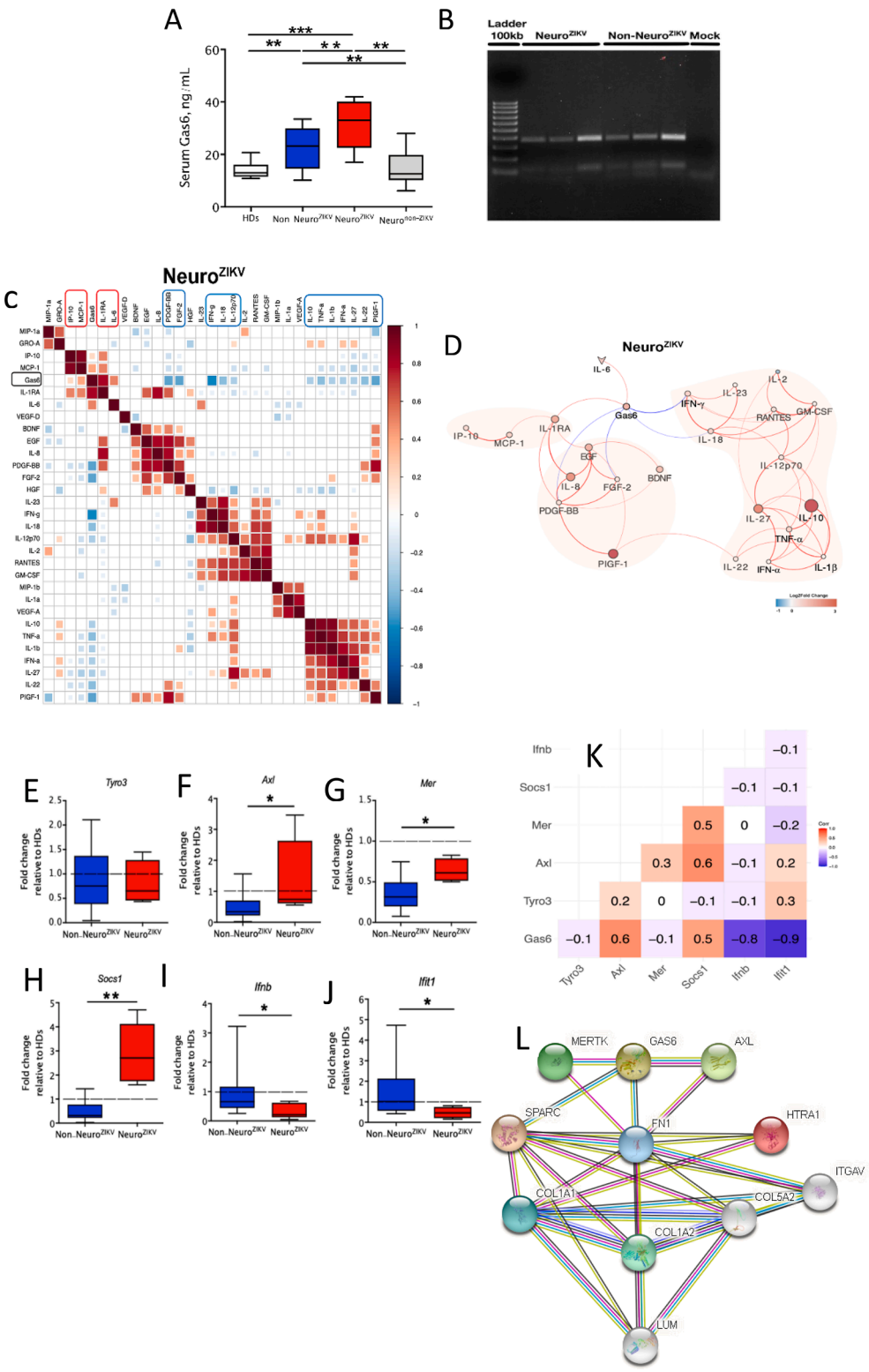

Fig. 3. Elevate Gas6 levels in Neuro^{ZIKV} patients is a ZIKV-specific response associated with immune signatures related to disease manifestation. (A) Levels of Gas6 in acute-phase patient serum samples of Zika virus (ZIKV) cross-sectional cohort in Campinas, Brazil, were determined by ELISA: Healthy donors (HDs, n = 13), ZIKV patients without neurological complications (Non-Neuro^{ZIKV}; n = 57), patients with neurological complications (Neuro^{ZIKV}; n = 19) and patients presenting neurological complications unrelated to ZIKV infection (Neuro$^{NON-ZIKV}$; n = 14). Gas6 concentration is depicted as Tukey box plots. Kruskal-Wallis test with post hoc correction for multiple testing using the original FDR method of Benjamini and Hochberg were conducted. *$p < 0.05$; **$p < 0.01$; ***$p < 0$ 0.001. (B) Identification of *GAS6* 834 + 7AA genotypes in ZIKV-infected patient groups by agarose gel electrophoresis. Lane 1: Ladder 100 kb size marker. Lanes 2–4: Neuro^{ZIKV}; Lanes 5–7: Non-Neuro^{ZIKV}; Lane 8: Mock. AA homotype showing 345 and 136 bp bands. (C, D) Representative images of Pearson's correlation matrix calculated for each clinical group. A reduced complexity model was established by focusing on informative interactions between ZIKV-specific immune signatures and Gas6 determined by Pearson's correlation coefficients. Only correlations with associated *p*-value < 0.05 are shown and hierarchical clustering was applied. (D) Representative images of the networks of interactions (prefuse-force layout). Each connecting line (edge) represents a significant interaction ($p < 0.05$ and $r \geq 0.5$) calculated by the network analysis using the R software. Edge weights and colour are defined as the correlation strength; positive correlations are represented by red edges; negatives correlations are represented by blue edges. Node colour and size represent Log_2 Fold Change of each biomarker normalized by baseline levels in healthy donors. Quantitative mRNA expression was determined in peripheral blood cells isolated from healthy donors (HDs) and ZIKV-infected adult patients with (Neuro^{ZIKV}) and without neurological complications (Non-Neuro^{ZIKV}) by qRT- PCR. (E) *TYRO3*; (F) *AXL*; (G) *MER*; (H) *SOCS1*; (I) *IFNb*; (J) *IFIT1*. Graphs depict fold change calculated relative to healthy donor samples (dashed line) as Tukey box plots, after results were normalized to GAPDH housekeeping gene expression. A student's *t*-test was used to compare groups with normally distributed data, and a Mann-Whitney test was used to compare groups with non-normal distributions; *$p < 0.05$; **$p < 0.01$. (K) Spearman's Rank Correlations were determined to assess the association between levels of Gas6 in the serum and expression levels of the transcripts quantified in the matched peripheral blood cells form ZIKV-infected adult patients. (L) Correlation obtained from STRING database without any input for Gas6 protein network. (For interpretation of the references to colour in this figure legend, the reader is referred to the web version of this article.)

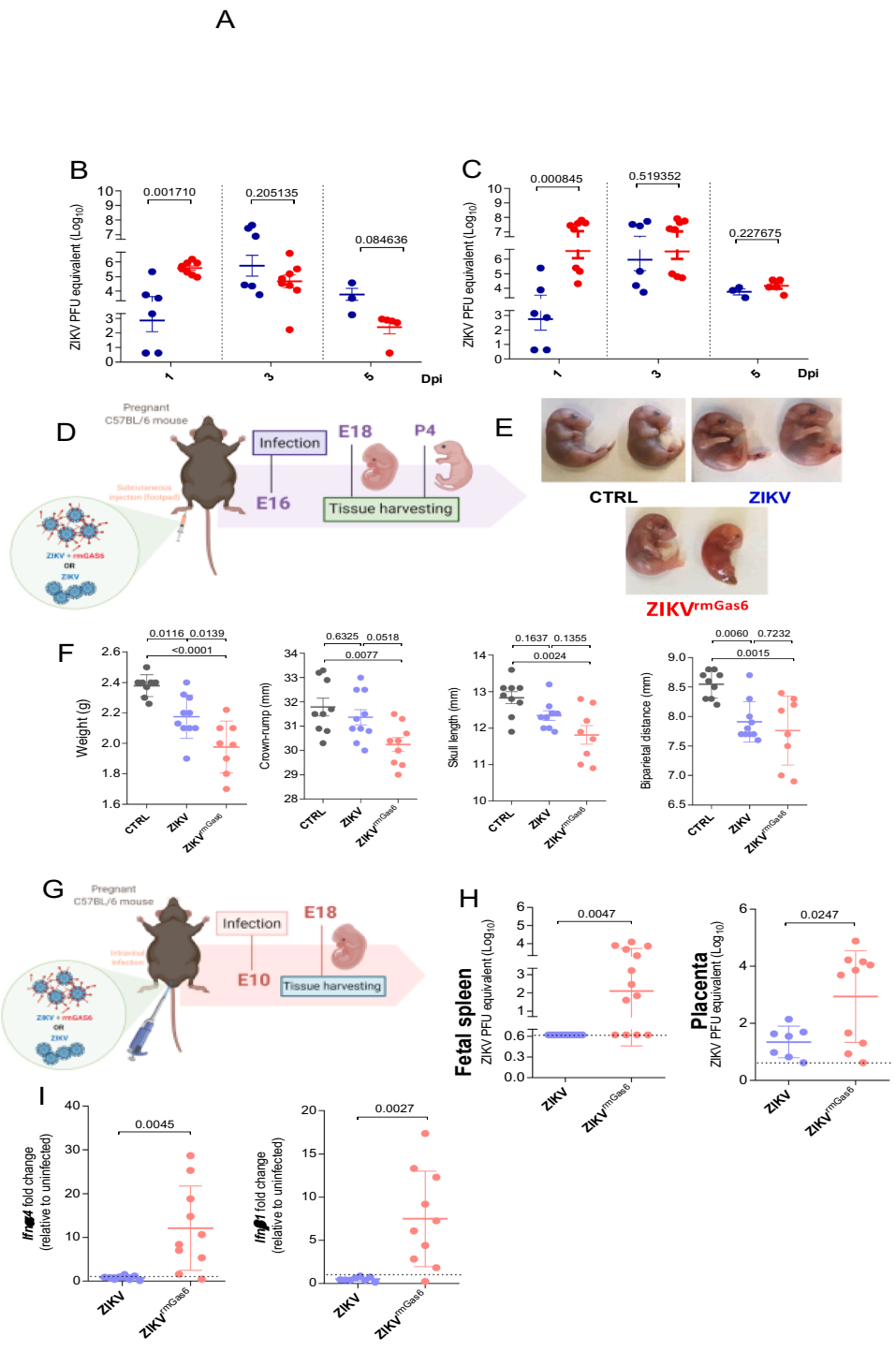

Fig. 4. Gas6 facilitates ZIKV replication and promotes ZCS and transplacental infection in ZIKV-infected resistant immunocompetent mice. SJL and C57BL/6 mice were infected by intravenous route with 10^2 pfu of pure ZIKV (BeH815744) or ZIKV previously incubated with rmGas6 (1 μg/mL) ($ZIKV^{rmGas6}$) (A). After 1-, 3- and 5-days post-infection the viral load was analysed by qPCR in spleen of SJL (B) and C57BL/6 (C) mice strains. The significances between ZIKV and $ZIKV^{rmGas6}$ in each time point of viral load was measured by multiple Student's *t*-test *p*-values < 0.05 were considered significant. Graphs shown are representative of three independent experiments; 1 and 3 dpi: ZIKV (n = 6), $ZIKV^{rmGas6}$ (n = 8); 5 dpi: ZIKV (n = 3), $ZIKV^{rmGas6}$ (n = 5). Pregnant mice were infected subcutaneously with pure ZIKV (10^5) or ZIKV previously incubated with rmGas6 (1 μg/mL) ($ZIKV^{rmGas6}$) on E (embryonic day) 16. The organs were harvested on E18 or postpartum day (P) 4 (D). The viral load was analysed by qPCR. Foetus's macroscopic analysis at E18 (E). Dimension analyses at P4 (F). Pregnant mice were also infected intravaginally on E10 with pure ZIKV (10^5) or ZIKV previously incubated with rmGas6 (1 μg/mL). Tissues were harvested at E18 (G). Viral load in spleen and placenta (H). Gene expression in placenta (I). Fold change was calculated between uninfected and infected groups. The significances between the groups were performed by One-way ANOVA (c) and Student *t*-test (d, f and g), *p*-values < 0.05 were considered significant. Graphs shown are representative of two independent experiments. Numbers of experimental groups: (F) Control n = 8; ZIKV n = 10; $ZIKV^{rmGas6}$ n = 8. (H) Control n = 6; ZIKV n = 11; $ZIKV^{rmGas6}$ n = 14. (I) Control n = 6; ZIKV n = 11; $ZIKV^{rmGas6}$ n = 9.

As Axl is expressed in decidua, Hoffbauer, trophoblast and fibroblasts cells of human placenta and ZIKV has been considered a sexually transmitted disease (STD), we sought to verify whether Gas6 facilitates intra-uterine ZIKV infection. For that, C57BL/6 pregnant mice were intravaginally infected at E10 with ZIKV or $ZIKV^{rmGas6}$ and viral load was determined at E18 (Fig. 4G). Contrasting with the subcutaneous infection, macroscopic changes were not observed at E18 (Supp Fig. 8F, G), but there was also a significant increase in ZIKV load in the foetal spleen and in the placenta of $ZIKV^{rmGas6}$-infected pregnant mice (Fig. 4H). Although we see no change in *Stat1* and *Socs1* mRNA expression, *Ifnα4 and Ifnβ1* expression were unexpectedly increased in the placenta of $ZIKV^{rmGas6}$-infected pregnant mice (Fig. 4I) contrasting with type I IFNs expression in E18 foetal placenta in which the gene expression is not upregulated (Supp. Fig. 8D).

3. Discussion

The ZIKV epidemic that started in 2015 was a great public health problem. ZIKV can cross the blood–brain and placental barriers, infecting the central nervous system (CNS) of adults and developing foetuses, greatly increasing the severity of the clinical outcomes (Miner et al., 2017; Yuan, et al., 2017; Cugola, et al., 2016; Russo et al., 2017;

Rasmussen et al., 2016; de Araújo, et al., 2018; Soares de Oliveira-Szejnfeld, P., et al., Congenital Brain Abnormalities and Zika Virus: What the Radiologist Can Expect to See Prenatally and Postnatally. Radiology, et al., 2016; Proenca-Modena, et al., 2018). In fact, studies with *ex vivo* slices from human cortical tissue and adult mice demonstrated that ZIKV infect and replicate in mature neurons, causing local inflammation and damage in hippocampal synapses, resulting in impairment of synaptic function and memory (Figueiredo, et al., 2019). These findings show that contemporary occurring ZIKV strains are highly neurotropic and detrimental to both mature as well as to the developing central nervous system (CNS) (Yuan, et al., 2017; Souza et al., 2019). Although studies have raised the contribution of several factors in the development of these conditions (Cugola, et al., 2016; van den Pol, et al., 2017; Wu, et al., 2016), the mechanisms by which the virus reaches the brain of adult individuals is not fully understood. In this context, here we demonstrate of Gas6 may have an important role and that increased circulating levels induced by the virus may worsen clinical outcome and, for instance, resulting in neurological complications. This upregulation is ZIKV-specific and could be influenced by intrinsic host features such as allelic variability of the human *GAS6* gene. Elucidation of the human *GAS6* gene structure and allelic variants revealed the presence of eight different variants confirmed to be single nucleotide polymorphisms (SNPs). The SNP in the intron 8 (c.834 + 7G > A; genotypes GG, AG, and AA) controls circulating levels of Gas6 and plays a key role in the pathogenesis of different circulatory disease, such as preeclampsia, acute coronary syndrome and stroke (Ozakpinar, et al., 2016; Jiang, et al., 2009; Muñoz, et al., 2004; Muñoz, 2007). We observed no difference in *GAS6* haplotypes, as both groups of patients showed the predominant frequency of the c.834 + 7G > A;AA genotype, indicating that higher Gas6 levels observed in Neuro^{ZIKV} patients correlate to ZIKV infection.

Different from hBMECs, monocytes were more responsive to ZIKV infection by upregulating transcriptional and translational machinery resulting in the increase of Gas6 expression. This indicates that monocytes might be the main cellular source and contributing to increased Gas6 levels in the plasma of ZIKV-infected patients. It is worth mentioning that this is consistent with the fact that circulating CD14^{+}CD16^{+} monocytes carry ZIKV particles during infection (Foo, et al., 2017; Michlmayr, et al., 2017). Moreover, in immune cells, engagement of TAM receptors by Gas6 results in the inhibition of inflammatory responses driven by Toll-like receptors (TLR) and type I IFN signalling pathways (Alciato, et al., 2010; Zhao, et al., 2017; van der Meer and van der Poll, 2014; Lemke and Rothlin, 2008; Rothlin et al., 2007). The mechanism depends on the expression of SOCS, resulting in an autocrine and paracrine inhibition of both signalling pathways during ZIKV infection *in vivo*. This response in leukocytes, particularly in monocytes, and microvascular endothelial cells might contribute to virus spread and replication in the periphery and potentially in target tissues, such as the CNS. Therefore, our network analysis of associations between Gas6 and ZIKV-specific immune signatures and transcriptional profiling of peripheral blood cells further elucidate the pathogenic mechanism of action of Gas6. Different from healthy donors, the increase of Gas6 levels in Non-Neuro^{ZIKV} patients changes its patterns of correlations, and we have found a significant positive correlation between Gas6 and IFN-α. This, along with increased circulating levels of proinflammatory cytokines, chemokines and growth factors, suggests that an active production of a network of immune mediators could provide a strong antiviral environment during the acute phase of disease, resulting in a milder clinical outcome. Conversely, in Neuro^{ZIKV} patients, the further increase of Gas6 expression changes its pattern of interactions. Gas6 displays a positive correlation with IL-6, MCP-1, IP-10, IL-1RA and negative correlations with IFN-α, IFN-γ and IL-18, important antiviral cytokines. In addition, as shown in the network graph, as IFN-γ forms a functional cluster with a variety of important mediators in host defense against infection (Kam et al., 2017; Chaix, et al., 2008), Gas6 also displays indirect negative correlations with TNF-α, IL-1β, IL-12, IL-22 and IL-27. This pattern of interactions reveals that elevation of circulating Gas6 levels above a certain threshold, which we estimate to be higher than 30 ng/mL, dampens the protective immune response that provide a strong antiviral environment and a milder clinical outcome. In support, transcriptional analysis in peripheral blood cells from ZIKV patients with neurological complications indicate that this response is achieved by a ZIKV–Gas6–TAM receptor interaction that ultimately induces downregulation of type I IFN genes modulated by SOCS1. This mechanism was corroborated in cultured monocytes, where ZIKV-induced Gas6 expression also correlated with suppression of type I IFN response.

The antiviral response also involves recruitment and coordination of specific subsets of immune cells orchestrated primarily by chemokines. Gas6 can also function as an inflammatory molecule by inducing leukocyte adhesion on endothelial cells surface and extravasation through a P-selectin–dependent mechanism (Tjwa, et al., 2008). Moreover, Axl and Mer, in cooperation with IFNAR signalling, have been described as key molecules for maintenance of the BBB and protection to WNV and La Crosse virus infection (Miner, et al., 2015). Accordingly, *in vivo* studies of ZIKV infection in immunocompromised IFNAR-KO mice lacking Axl have shown protection from ZIKV neuropathogenesis and severe infection (Hastings, et al., 2019). In this context, suppression of IFNAR signalling due to increased amounts of circulating Gas6 in Neuro^{ZIKV} patients have the potential to impair BBB homeostasis and integrity. This may allow viral and cellular extravasation to CNS through loose endothelial cells junctions. Noteworthy, in Neuro^{ZIKV} patients, Gas6 positively correlates with IL-6, IP-10 and MCP-1, suggesting that there might be a parallel between ZIKV and cytokine release syndrome (CRS). In addition, our data reveal a unique and inappropriate inflammatory response in Neuro^{ZIKV} patients. This response is defined by a failed type IFN-I response in the periphery, juxtaposed to elevated chemokines levels and high expression of IL-6, leading to recruitment and infiltration of effector immune cells in deep tissues. Thus, infiltration of cells, such as CD4 and CD8 T cells, along with infection of mature neurons could induce a local inflammatory response in the CNS, potentially resulting in neurological complications (Figueiredo, et al., 2019). We propose that Gas6 mediated reduced innate antiviral defences coupled with exuberant inflammatory cytokine production are driving features of severe clinical outcome in ZIKV adult patients.

It has been shown that inhibition of Axl signalling by different pharmacological or genetic approaches decrease ZIKV replication *in vitro* in CNS cells, endothelial cells and dendritic cells as well as reduce brain pathology in experimental models (Meertens, et al., 2017; Hastings, et al., 2019; Richard, et al., 2017; Liu, et al., 2016; Bowen et al., 2017). TAM receptors activation by Gas6 is highly dependent on its γ-carboxyglutamic acid-rich (Gla) domain, required for its biological activity and to bridge enveloped viruses to bind and activate TAM receptors (Davra et al., 2016; Meertens, et al., 2012; Bhattacharyya, et al., 2013; Perera-Lecoin, et al., 2013; Nakano, et al., 1997). After translation, Gas6 is activated by γ -glutamyl carboxylation via the Vitamin-K cycle (Davra et al., 2016). Vitamin-K epoxide reductase enzyme complex 1 (VKORC1) recycles Vitamin-K Epoxide back to Vitamin-K Hydroquinone, which in turn serves as a co-factor in the γ-carboxylation of Gas6 induced by Vitamin-K-dependent enzyme γ-glutamyl carboxylase (GGCX). Low-dose of warfarin functions as a direct VKORC1 inhibitor, preventing γ-carboxylation of Gas6 and TAM receptor activation (Davra et al., 2016; Kirane, et al., 2015). Thus, we used low-dose warfarin to further determine the mechanistic link between Gas6 production, ZIKV replication and suppression of antiviral response. It is important to highlight that one could argue that decreased Gas6 production after warfarin treatment could be a result of decreased binding of anti-Gas6 capture antibody in the ELISA due to restricted recognition of γ-carboxylated residues (amino acids 53–92) in Gas6 protein. However, the capture antibody recognizes the residues 118–678, which are not in the Gla-domain. In addition, Gas6 can be transcriptionally upregulated by Axl-mediated autocrine mechanisms (Davra et al., 2016), which

could explain warfarin-induced downregulation of Gas6 expression. In our experiments, this mechanism was confirmed by restoration of antiviral response and complete blockage of production of infective viral particles when monocytes were treated with warfarin. These findings implicate that, by tethering ZIKV to TAM receptors, Gas6 mediates the pivotal suppression of type I interferon receptor (IFNAR) signalling, thereby favouring ZIKV evasion from antiviral immunity and sustained replication, pointing out how interactions with membrane receptors go beyond attachment and internalization of viral particles (Oliveira and Peron, 2019).

We demonstrate a correlation between Gas6 protein expression, ZIKV RNA load and production of infecting particles associated with suppression of type I IFN response in human cells infected *in vitro*. Although we did not detect difference in ZIKV RNA load in the peripheral blood specimens in our cross-sectional cohort, this could probably be due to the moment blood sampling was performed. When immunocompetent adult C57BL/6 and SJL mice were infected with Gas6-coated ZIKV ($ZIKV^{rmGas6}$), we observed that upregulation of Gas6 increased viral load very early, at 1 d.p.i. After 3 and 5 d.p.i, differences were no longer detected. This might explain our observation in patients, as the median interval between illness onset and sampling was 4 days, ranging from 1 to 6 days. Thus, similar to *in vitro* infection of cultured human cells, these data corroborate the role of Gas6 in increasing ZIKV replication *in vivo*. Intriguingly, some studies that also used *in vivo* experimental approaches have demonstrated that the presence of TAM receptors are not required for ZIKV infection in the testis, eye, brain and neither for transplacental infection (Ma, et al., 2017; Miner, et al., 2016; Hastings, et al., 2017). Nevertheless, our data are the first to describe that Gas6 facilitates ZIKV replication in adult immunocompetent mice model acting as a gatekeeper for viral entry. In addition, these observations corroborate *in vitro* studies of ZIKV and DENV infection (Meertens, et al., 2017; Meertens, et al., 2012).

We had previously evidenced the resistance of C57BL/6 mice to congenital malformations caused by ZIKV (Cugola, et al., 2016). Here, we demonstrated that Gas6 could render C57BL/6 susceptible to ZIKV induced growth restriction and viral transplacental passage associated with increased placenta *Ifnα* and *Ifnβ* expression. Axl is expressed in decidua, Hoffbauer, trophoblast and fibroblasts cells of human placenta, suggesting as the receptor viral transplacental passage (Yockey et al., 2018). Interestingly, recent studies have demonstrated that CZS is associated with exacerbated type I IFN and insufficient type III IFN in placenta at term, probably without modulation of TAM or TIM receptor mRNA expression in placental sites infected with ZIKV (Azamor, 2020; Nobrega, et al., 2020). In addition, human babies carrying CG/CC genotypes of rs2257167 in IFNAR1 presented higher risk of developing CZS (Azamor, 2020). However, the correlation between TAM receptors and Gas6 expression in susceptibility to congenital ZIKV syndrome has not been established. Our data also demonstrate that intravaginal infection with Gas6-coated ZIKV leads to increased viral load in the placenta of pregnant mice and in the spleen of their foetuses, pointing out the role of Gas6-TAM receptors for transplacental passage. Supporting these results, previous studies have demonstrated that placental viral infection is capable to elicit morphological changes in the foetal brain associated with IFN-β immune response at the maternal-foetal interface (Yockey et al., 2018). Interestingly, deficient *Ifnar* mice, despite higher viral load, do not present significant impairment in the offspring development. However, those who type I IFN response was present ($Ifnar^{+/-}$), despite lower viral load, demonstrated placental spiral arteries apoptosis, foetal hypoxia and prominent growth restriction. In the same study, intraperitoneal injection of poly: IC, a major TLR3 agonist which is also activated by ZIKV (Dang et al., 2016); led to resorption of all foetuses in an IFNAR-dependent manner (Yockey et al., 2018). Accordingly, the hypothesis for our findings would be that the immunocompetence described in C57BL/6 animals may be beneficial while low amounts of pathogen are present. However, if viral load is increased, as it happens due to infection with $ZIKV^{rmGas6}$, the exacerbated immune response in the pregnant mother could result in detrimental changes to foetal development probably resulting from increased placental damage.

Regarding the role of Gas6 as a procoagulant molecule that could affect fetal development, we discarded that the malformations may be due to exogenous Gas6 since *in vivo* administration of recombinant Gas6 only affects artificial-induced thrombosis. Additionally, the amounts of Gas6 used in this study are very low in comparison with previous studies with the ligand.

Together, our observations in ZIKV-infected adult patients and *in vitro* infections identify a relevant pathogenic mechanism associated to the development of severe outcomes during ZIKV infection, where the virus promotes upregulation of its own ligand Gas6, which contributes to viral infectivity by suppressing an efficient type I IFN antiviral response (Fig. 5A and B). Our *in vivo* findings in immunocompetent mice models corroborate the role of Gas6 for favouring ZIKV infection by acting as a gatekeeper in addition to its association with the pathogenesis of congenital syndrome (Fig. 5C). Interestingly, the correlation of Gas6 plasma levels and disease severity has already been described in lupus (Gong, et al., 2019), liver fibrosis (Smirne, et al., 2019) and preeclampsia (Peng, et al., 2018). To our knowledge, our work is novel in linking the importance of Gas6 both in human subjects and experimental models. This contributes not only to a better understanding on the pathogenesis of ZIKV infection and severe clinical outcomes, but also open new avenues that target Gas6 as a therapeutic tool.

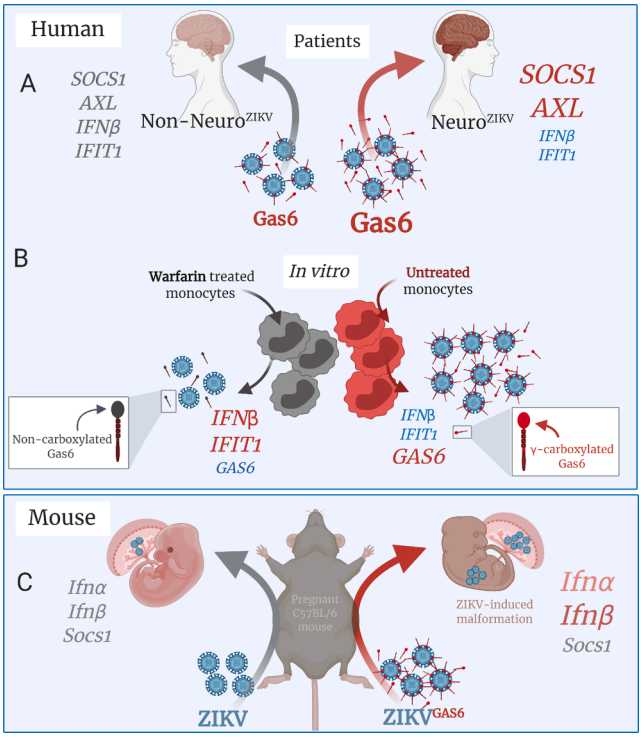

Fig. 5. Gas6 is associated with neurological complications in humans and drives ZIKV-congenital malformations in immunocompetent mice. (A) Elevated Gas6 levels in the serum of ZIKV patients with neurological complications (Neuro ZIKV) is associated with upregulation of AXL and SOCS1 and downregulation of IFNβ and IFIT1. (B) In vitro treatment with Warfarin reduces Gas6 levels and restores type I IFN antiviral response by inhibiting Gas6 γ-glutamic acid carboxylation thus decrease ZIKV infection. (C) The mouse infection with ZIKV pre-treated with recombinant Gas6 (ZIKV Gas6) facilitates Zika virus infection and leads to malformations in the offspring which is associated with upregulation of Ifnα and Ifnβ. Created by the authors with *www.BioRender.com*.

4. Materials and methods

4.1. Ethical approval

The present study was conducted according to the Declaration of Helsinki principles after approval by the Research Ethics Committee of the University of Campinas (CAAE: 56793516.0.0000.5404) (Kam et al., 2017). Written informed consent was obtained from all participants or from participants' parents / legal guardians. In addition, animal experiments were carried out in accordance with the recommendations of the IACUC (Institutional Animal Care and Use Committee). The protocols were approved by Ethics Committee for Animal Research of University of Sao Paulo (CEUA – 63/2016) and all efforts were made to minimize animal suffering.

4.2. Patients

This was a cross-sectional study that enrolled 90 patients and 13 healthy donors during the Zika virus (ZIKV) epidemic in Brazil. The patients were admitted to hospitals through emergency departments (ED) in the city of Campinas, Southeast of Brazil, during the ZIKV outbreak (February 2016 to June 2017). 57 of these 90 patients had a mild self-limited illness by ZIKV, characterized by the presence of the following symptoms: fever, rash, conjunctivitis, myalgia, headache, arthralgia and periarticular edema, while 33 patients had clinical signs compatible with neurological syndromes, 19 with diagnosis of ZIKV and 14 without ZIKV detection. This study included patients presenting clinical diagnosis of encephalitis, meningoencephalitis, transverse myelitis and Guillain-Barré syndrome of undetermined origin that had preceding symptoms compatible with arbovirus infection up to 60 days before the onset of the neurological condition. The clinical classification was done following international clinical criteria (Kalita et al., 2008; Venkatesan et al., 2013) and patients with history of a prior motor neuropathy or spinal cord disease were excluded of the study. Clinical data were retrospectively retrieved from medical records and the clinical and demographics data are summarized in the Table 1 in the main text. Patients included in this study were grouped as follows:

Patients ZIKV^{+} with mild symptoms (Non-Neuro^{ZIKV})*:* 57 patients presenting mild symptoms of infection, such as low fever, rash, myalgia and conjunctivitis. ZIKV infection was confirmed by qRT-PCR.

Patients ZIKV^{+} with neurological complications (Neuro^{ZIKV})*:* 19 patients presenting neurologic complications secondary to ZIKV were diagnosed with Guillain-Barré syndrome, encephalitis, meningitis, meningoencephalitis or transverse myelitis according to clinical criteria. Neurological complications started at a median of 4 days after onset of ZIKV acute symptoms. ZIKV infection was confirmed by qRT-PCR and/or specific IgM detection,

Patients ZIKV^{-} with neurological symptoms (Neuro$^{NON\text{-}ZIKV}$)*:* 14 patients presenting neurologic complications as described above but were negative for ZIKV by qRT-PCR and/or specific IgM detection. Although three of these patients were positive for DENV by NS1/IgM Rapid immunochromatographic tests, the pathological origin of these neurological symptoms was undetermined at the moment of sample collection. All these patients were negative for DENV, CHIKV and OROV by qRT-PCR.

Healthy donors (HDs): 13 age-matched individuals without signs of infection within 30 days prior to sample collection. They were included and pre-screened for presence of ZIKV RNA and ZIKV-specific antibodies.

Additionally, not included in the 90 described patients, we analysed acute-phase serum samples of 8 ZIKV-infected pregnant women and 6 infants born of these women. Of these infants, two had CNS abnormalities associated to Congenital Zika Syndrome (CZS), while 4 infants were healthy, without congenital zika syndrome (Non CZS). All participants were tested for a series of arboviruses by qRT-PCR. All patients and healthy donors were negative to Dengue (DENV), Chikungunya viruses (CHKV) and Oropouche were negative as determined by RT-qPCR. Samples were collected after consent of the patients.

Serum Collection and Processing: Peripheral blood and/or urine specimens were collected at a median of 3 days post-illness onset. Serum was obtained from 10 mL of peripheral blood collected in a dry heparinized tube after peripheral venepuncture. All samples were transported and processed as previously described (Kam et al., 2017). Positivity ZIKV RNA in the blood, serum and urine samples was verified by real-time quantitative RT-PCR (qRT-PCR) (Kam et al., 2017; Judice, et al., 2016). In addition, the presence of ZIKV-specific IgM and IgG antibodies in the serum was determined by enzyme-linked immunosorbent assay (ELISA), as previously described (Kam et al., 2017; Judice, et al., 2016).

4.3. Cells:

This study was conducted using the following cells lines: Vero E6 (ATCC®, (Manassas, Virginia, USA) CRL-1586™), C6/36 (ATCC® CRL-1660™), THP-1 (ATCC® TIB-202™) and hBMECs (previously described here (Nikolskaia, et al., 2006) and kindly provided by Dr. Julio Scharfstein – Instituto de Biofísica Carlos Chagas Filho, UFRJ). VeroE6 were cultured in DMEM medium (high glucose) supplemented with 10% fetal bovine serum (FBS). mosquito cell line were cultured in Leibovitz's L-15 medium supplemented with 10% FBS and 1% penicillin/streptomycin. Human brain microvascular endothelial cells (hBMEC) were cultured in DMEM high glucose, supplemented with 1% L-glutamine, 1% non-essential aminoacids, and 10% FBS (Papa, et al., 2017). Peripheral blood mononuclear cells (PBMC) from healthy donors were obtained after centrifugation of buffy coat samples over ficoll-hypaque gradient. Subsequently, the mononuclear cell ring was collected and washed with 1x PBS, followed by centrifugation. Then, the pellet was resuspended in complete RPMI-1640 (supplemented with 10% FBS and 1% antibiotics). Cells were then counted for determination of cell viability by Trypan Blue. PBMCs and THP-1 human monocytic cell line were maintained in a complete RPMI-1640 medium supplemented with 10% FBS, 2 mM L-Glutamine (Corning), and 1x Penicillin-Streptomycin Solution at 37 °C in a fully humidified atmosphere containing 5% CO_2.

4.4. Virus strains

For *in vitro* studies in cultured human cells, Brazilian ZIKV strain (BeH823339, GenBank KU729217), originally isolated from a patient in Ceará, Brazil in 2015, was provided by Professor Edison Durigon (Biomedical Sciences Institute, University of São Paulo, Brazil). Virus stocks were produced by inoculating Vero CCL81 cells (ATCC) with ZIKV in minimum essential medium (MEM) for 2 h at 37 °C and 5% CO_2. Further, the supernatant was removed, and MEM supplemented with 2% FBS, 1% penicillin and streptomycin was added. The cells were incubated for 4 days until 70% of cytopathic effect. Supernatant was then collected, centrifuged for 5 min at 10,000g, 4 °C and snap-frozen at −80 °C until use.

For *in vivo* studies in mice, Brazilian ZIKV (BeH815744, GenBank KU365780) was provided by Evandro Chagas Institute in Belém, Pará, Brazil and propagated in C6/36 cells. Cultures were infected for 1 h at 27 °C in the absence of CO_2. Further, 45 mL of complete medium was added (2% of FBS + 1% of Pen/Strep) and cultures were followed until reaching cytopathic effect. At this time, supernatants were harvested and centrifuged at 3200 rpm for 10 min at 4 °C to remove any detached cell. ZIKV culture supernatants were further precipitated with 50% of PEG (polyethylene glycol) for 18 h at 4 °C. Precipitated virus supernatants were centrifuged (30′, 3200 *g*, 4 °C), and the pellet was diluted in DMEM with 25 Mm HEPES quantified by PFU assay in VERO cells and used as necessary.

4.5. Mice

SJL and C57BL/6 mice were bred under specific-pathogen-free conditions at University of São Paulo animal facility of the Department of Immunology - ICB. 8-week-old non-pregnant or 11-week-old pregnant female mice were used. All animals were maintained in accordance with institutional guidelines for animal welfare after approval by the Institutional Animal Care and Use Committee at University of São Paulo, as described above.

4.6. ZIKV real-time quantitative RT-PCR

Viral RNA from blood, serum or urine samples was extracted using the easyMAG mated extractor (BioMerieux, Quebec, Canada) or QIAamp viral RNA mini kit (Qiagen, Hilden, USA), according to manufacturer's instructions. Estimation of viral RNA copy number in patients' samples was performed using real-time RT-PCR (TaqMan RNA to-Ct 1-Step Kit; Applied Biosystems) with primers and probes, as previously described (Kam et al., 2017; Kalita et al., 2008). qRT-PCRs with cycle threshold (Ct) values higher than 40 cycles were considered negative. Quantitative assay was performed using a standard curve produced with serial 10-fold dilutions of ZIKV RNA expressed on a log10 scale as genome equivalents/sample.

4.7. Viral RNA sequencing and assembly

To evaluate the quantity and quality of the RNA extracted, a Qubit® 2.0 Fluorometer (Invitrogen, Carlsbad, USA) and an Agilent 2100 Bioanalyzer (Agilent Technologies, Santa Clara, USA) were used, respectively. Synthesis of cDNA was performed using SuperScript II and random hexamer primers according to the manufacturer's recommendations (Invitrogen, Carlsbad, USA). Nucleotide sequencing was performed using the TruSeq RNA sample preparation kit in an Illumina HiSeq 2500 instrument (Illumina, San Diego, USA) with a paired-end and 150-base-read protocol in *RAPID* module. The sequencing reads were assembled *de novo* using the metaViC pipeline (available on https://github.com/sejmodha/MetaViC), as previously described (Souza, et al., 2018).

4.8. Viral quantitation by focus forming unit assay and plaque forming unit assay

The viral titter of viral isolates was determined by both focus forming unit (FFU) and plaque forming unit (PFU) assays in Vero E6 cells. The quantitation of viral load during *in vitro* experiments were performed by FFU assay, while the viral load in different tissues of animals were determined by PFU assay. For FFU quantification, samples were clarified by centrifugation (2,000 × g at 4 °C for 10 min) and diluted serially prior to infection. These dilutions were added to Vero E6 cells in 96-well plates for 2 h for viral adsorption and, after supernatants removal, cells were maintained with MEM + 1% CMC medium (final concentration) supplemented with 5% FBS and 1% penicillin/streptomycin for 48 h at 37 °C and 5% CO_2. The overlay was removed, and cells were fixed overnight with 1% paraformaldehyde (PFA) in PBS. To detect infected cell foci, cells were permeabilizated with Triton buffer (PBS 0.15 M, 0.1% BSA and 0.1% Triton X-100) and foci were detected after incubation with a mouse anti-ZIKV NS1 antibody in a volume of 50 µl for 2 h at room temperature. After three washes with 300 µl of permeabilization-wash buffer (P-W; PBS, 0.1% saponin, and 0.1% bovine serum albumin [BSA]), the samples were incubated with 50 µl of a 1:2,000 dilution of horseradish peroxidase (HRP)-conjugated goat anti-mouse IgG for 1 h at room temperature. Focci were stained by the addition of the TrueBlue detection reagent (KPL), and the blue spots were counted after three washes with distilled water.

For PFU quantification, Vero E6 cells (1×10^5/well) distributed in 24-well plate were culture with clarified samples from infected mice. These samles were diluted ($10^5 - 10^1$) in RPMI-16–40 medium and used to infect VeroE6 cells for 1 h at 37 °C. Further, supernatants were removed and DMEM medium (2% FBS + 1% penicillin/streptomycin) + 1.5% CMC (Carboxymethyl cellulose) were added in each well. Cells were cultured in 37 °C for 5 days and then stained with crystal violet for plaque counting. Viral titter of the stock sample was determined by: [average number of plaques/ (dilution factor of well)] × (volume of inoculum per plate).

4.9. ZIKV infection and treatment

For *in vitro* infection, PBMCs, THP-1 monocytes and hBMECs were infected with ZIKV MOIs (multiplicity of infection) ranging from 0.1 to 10, depending on the experimental design. In some experiments, cells were submitted to starvation (serum free medium) from 4 to 18 h prior to infection with the virus for 2 h at 37 °C. Afterwards, cells were washed four times with PBS. Culture medium was added to each well and the cells were incubated at 37 °C and 5% CO_2 for the duration of the experiment. For Gas6 γ-carboxylation and Axl kinase blockade experiments, cells were incubated or not (mock) with 2 µM warfarin or 2 µM R428 (BerGenBio), respectively. Cells were harvested after 1-, 2-, 3-, 4-, 6-, 9-, 12-, 24-, 48- or 72-hours post infection depending on the experimental design. Medium was harvested at specified time points for determination of Gas6 production, ZIKV titters and replication either by PFU or flow cytometry.

4.10. Mice infection

For *in vivo* experiments in mice, the BeH815744 virus was incubated or not with 1 µg/mL of recombinant mouse Gas6 (rmGas6) in µl for 4 h at 37 °C prior to mice inoculation (Morizono, et al., 2011). 8-week-old SJL or C57BL/6 wt mice were inoculated with 10^2 ZIKV pfu diluted in 100 µl of PBS or pre-incubated with 1 µg/mL of recombinant murine Gas6 ($ZIKV^{rmGas6}$) by intravenous route (retroorbital sinus). Mice were euthanized at days 1, 3 or 5 post infection depending on the experimental design. To study congenital infection, 11-week-old C57BL/6 wt pregnant mice were infected with ZIKV 10^5 pfu in 30 µl of PBS pre-incubated or not with 1 µg/mL rmGas6 at embryonic day E10 or E16 intravaginally or subcutaneously (footpad), respectively. Tissues were harvested at E18 or postnatally (P) at day 4.

4.11. Relative quantitation by Real-time quantitative RT-PCR:

For *in vitro* analysis, RNA was extracted using the miRVana miRNA Extraction kit (Ambion) according to the manufacturer's instructions. RNA quantity was determined by NanoDrop spectrometric dosing. Total RNA samples (up to 1 µg) were reverse transcribed using the oligo(dT) primer from the High-Capacity cDNA Reversion Transcription Kit (Thermo Fisher Scientific, Waltham, MA, USA). mRNA expression of the TAM receptors Tyro-3 (*Tyro-3*), Axl (*Axl*) and Mer (*Mer*), Suppressor of cytokine signalling-1/2 (*SOCS1*), Interferon-β (*IFN-β*), Interferon-induced protein with tetratricopeptide repeats-1 (*IFIT-1*), Gas6 (*Gas6*), Gamma-glutamyl carboxylase (*GGCX*), Vitamin K Epoxide Reductase Complex subunit 1 (*VKORC1*) and the housekeeping gene Glyceraldehyde 3-phosphate dehydrogenase (*GAPDH*) were determined by qRT-PCR, using iTaq Universal SYBR Green Supermix (Bio-Rad, Hercules, CA, USA). Cycling conditions were the following: 2 min at 95 °C and 35 cycles of 15 s at 95 °C and 60 °C for 1 min; 31 s at 65 °C and 60 cycles of 65 °C for 5 s (+0.5 °C/cycle; ramp 0.5 °C/s). The oligonucleotides used are described in Supplemental Table S1. Cycling conditions were the following: 95 °C for 5 min; 45 cycles of 95 °C for 15 s, and 60 °C for 1 min. The median cycle threshold (C_t) value and $2^{-\Delta\Delta Ct}$ method were used for relative quantification analysis and all C_t values were normalized to GAPDH. Results were expressed as means and SEM of biologic replicates. All qRT-PCR assays were performed on the CFX96 Touch™ Real-Time PCR Detection System (BioRad, Hercules, USA).

For *in vivo* analysis, RNA extraction from mice organs was performed according to the protocol provided by manufacturer TRIzol™ Reagent (Cat.No. 15596026). From the obtained RNA, we performed qRT-PCR according to the protocol provided by the manufacturer (Applied Biosystems Cat. No 4368813). The PCR reactions were done using TaqMan® gene expression assay with the following cycles 95 °C for 2 min and 45 cycles of 95 °C for 15 s and 60 °C for 1 min. Amplification was normalized by beta actin expression. Gene expression was analyzed by $2^{-\Delta\Delta Ct}$ method. Results were expressed as means and SEM of biologic replicates.

4.12. Flow Cytometry:

Vero E6 cells were incubated for 4 days with 72 h p.i. supernatants from THP-1 monocytes infected *in vitro* with ZIKV MOI 1, submitted or not to the different pharmacological treatments (mock, pre- or 2 h p.i. treatment with 2uM warfarin). Cells were fixed/permeabilized with Cytofix/Cytoperm (BD Biosciences, Franklin Lakes, New Jersey, U.S.) according to manufacturer's instructions and incubated with 1:100 mouse anti-ZIKV NS1 antibody at 4 °C for 30 min. Further, cells were washed with Permwash (BD Biosciences) and incubated with 1:100 Alexa Fluor 488-conjugated goat anti-mouse IgG H&L, washed and subjected to flow cytometry using a FACS Calibur (BD Biosciences). Flow data was analyzed with FlowJo V10.

4.13. ELISA for Gas6 quantification:

To measure Growth Arrest-Specific Protein 6 (Gas6) in patients' serum samples and supernatants from cells *in vitro*, ELISA was performed using Human Gas6 DuoSet ELISA kit according to the manufacturer's instructions (R&D Systems, Minneapolis, Minnesota, USA). Briefly, 96-well microplate was coated with the goat anti-human Gas6 capture antibody diluted to the working concentration in PBS and incubated overnight at room temperature. The plate was washed and incubated with blocking buffer (reagent diluent) at room temperature for 1 h After washing, samples were added (dilution 1:50 for serum samples and dilution 1:25 for cell supernatant samples) and incubated for 2 h. Next, plates were washed and biotinylated goat anti-human Gas6 detection antibody, diluted in blocking buffer was incubated for 2 h at room temperature, followed by streptavidin-HRP incubation for 20 min at room temperature. Plates were washed and incubated for 20 min with substrate solution. Optical density was determined at 450 nm followed by wavelength correction at 540 nm.

4.14. Single-nucleotide polymorphism of Gas6 (SNP):

Total DNA from patients' peripheral blood was extracted using QIAmp DNABlood Mini Kit (Qiagen, Germantown, Maryland, USA) following manufacture's instruction. Extracted DNA was used to perform PCR and electrophoresis analysis of the GAS6 Intron 8c.834 + 7G > A SNP, as previously described (Ozakpinar, et al., 2016). Reactions were performed using Taq DNA Polymerase Recombinant kit (Thermo Fisher Scientific, Waltham, Massachusetts, USA) following manufacture's recommendations. Thermocycling was as follows: 5 min at 94 °C, 35 cycles of 30 s at 94 °C, 30 s at 55 °C and 45 s at 72 °C, then followed by 5 min at 72 °C and 4 °C until digestion. Afterwards, amplicons were digested with restriction enzyme HhaI (New England Biolabs, Ipswich, Massachusetts, USA) at 37 °C for 4 h and separated in 1.5% agarose gel with ethidium bromide at 80 V for 90 min. UV documentation in Gel Doc XR + System (BioRad, Hercules, Califórnia, USA).

4.15. Correlation coefficients and network analysis:

Pearson's or Spearman's Rank correlation coefficients were determined to assess the association between Gas6 and ZIKV-specific immune signatures determined in the serum samples from healthy donors and ZIKV-infected patients by Multiplex Microbead-Based Immunoassay, as previously described (Kam et al., 2017). Correlation coefficients were also determined to assess the association between Gas6 levels in the serum and gene expression in the matched peripheral blood cells from ZIKV-infected adult patients. Correlations between transcripts were also quantified in the cells infected *in vitro* with ZIKV. For the network analysis, the systemic level of each biomarker was an input in the R software (v. 3.4.3). Along with the rank-order correlation coefficient, the p-value to test for non-correlation was evaluated using $p < 0.05$ as a cutoff. Next, correlation networks were generated by the analysis of relationships among each biomarker in the serum samples. Based on the correlation coefficients, the same software was applied to identify links (edges) of interactions between the biomarkers (nodes). The correlation strength is represented by edge transparency and width; positive correlations are represented by red edges, and negatives correlations are represented by blue edges. Following this approach, each biomarker was selected as a target, and the R software was used to perform a search within the other biomarkers for those that were associated with the target, in terms of correlation strength. As a result, the features related to the selected target were linked. This process was repeated for each biomarker, and the result was the inferred network among the input values. To analyze the structure of the networks, the graphs for the network analysis were customized in the Cytoscape software (v 3.5.1) using the pre-fuse force-directed layout. This layout follows an algorithm that in the equilibrium state for the system of forces, determined by the correlation strength, the edges tend to have uniform length, and nodes that are not connected by an edge tend to be drawn further apart

4.16. Statistical Analysis:

Data normality was checked by the Shapiro-Wilk test. Two-tailed Student's *t*-test or One-way analyses of variance statistical test with Bonferroni-corrected multiple comparisons test were used to compare means between groups with normally distributed data. Data sets with non-parametric distributions were compared using the Mann–Whitney test or Kruskal-Wallis test with post hoc correction for multiple testing using the original FDR method of Benjamini and Hochberg, with $p < 0.05$ considered significant. Data are presented as Tukey box plots or means and SEM, unless otherwise stated, of 2–3 representative and independent experiments with similar results. Analysis were performed and the graphs generated in GraphPad Prism 8 and R software. $p < 0,05$ were considered relevant.

CRediT authorship contribution statement

Joao Luiz Silva-Filho: Conceptualization, Methodology, Investigation. **Lilian G. Oliveira:** Conceptualization, Methodology, Investigation. **Leticia Monteiro:** Methodology, Investigation, Visualization. **Pierina L. Parise:** Methodology, Investigation, Visualization. **Nagela G. Zanluqui:** Methodology, Investigation, Visualization. **Carolina M. Polonio:** Methodology, Investigation, Visualization. **Carla L. Freitas:** Methodology. **Daniel A. Toledo-Teixeira:** Methodology, Investigation, Visualization. **William M. Souza:** Methodology, Investigation, Visualization. **Najara Bittencourt:** . **Mariene R. Amorim:** Methodology, Investigation, Visualization. **Julia Forato:** Methodology, Investigation, Visualization. **Stéfanie P. Muraro:** Methodology, Investigation, Visualization. **Gabriela F. Souza:** Methodology, Investigation, Visualization. **Matheus C. Martini:** Investigation, Visualization. **Karina Bispo-dos-Santos:** Investigation, Visualization. **Aline Vieira:** Investigation. **Carla C. Judice:** Methodology, Investigation, Visualization. **Glaucia M. Pastore:** Investigation. **Eliana Amaral:** . **Renato Passini Junior:** . **Helaine M.B.P. Mayer-Milanez:** . **Carolina C. Ribeiro-do-Valle:** . **Roseli Calil:** . **João Renato Bennini Junior:** . **Giuliane J. Lajos:** . **Albina Altemani:** . **Marcos T. Nolasco Silva:** . **Ana Carolina Coan:** . **Maria Francisca Colella-Santos:** . **Andrea P.B. Zuben:** . **Marco Aurélio R. Vinolo:** Investigation. **Clarice Weis Arns:** Investigation.

Rodrigo Ramos Catharino: Investigation. **Maria Laura Costa:** Visualization. **Rodrigo N. Angerami:** Visualization. **André R.R. Freitas:** Visualization. **Mariangela R. Resende:** Visualization. **Márcia T. Garcia:** Visualization. **Maria Luiza Moretti:** Visualization. **Laurent Renia: . Lisa F.P. Ng:** Investigation, Resources. **Carla V. Rothlin:** Resources. **Fabio T.M. Costa:** Conceptualization, Funding acquisition, Resources, Supervision. **Jean Pierre Schatzmann Peron:** Conceptualization, Funding acquisition, Resources, Supervision. **José Luiz Proença-Modena:** Conceptualization, Funding acquisition, Resources, Supervision.

Declaration of Competing Interest

The authors declare that they have no known competing financial interests or personal relationships that could have appeared to influence the work reported in this paper.

Acknowledgments

We thank the study participants and healthy volunteers for their participation and the clinical staffs from University of Campinas Hospitals and other hospitals of this city for assistance in patient enrolment and healthcare, blood sample preparation, study coordination, and data entry. We thank the staff of the Life Sciences Core Facility (LaCTAD) from Unicamp for the High-throughput sequencing.

Financial support.

This study was financially supported by the São Paulo Research Foundation (FAPESP 2016/00194-8; 2017/26170-0 and 2017/22054-1); Biomedical Research Council (BMRC; core research grants provided to the Singapore Immunology Network); the BMRC A*STAR-led Zika Virus Consortium Fund (project 15/1/82/27/001); the Agency for Science, Technology and Research (A*STAR), Singapore. J.L.S.F., L. G.O., L.M., P.L.P., N.G.Z., C.M.P., D.A.T.-T., W.M.S., N.B., J.F., S.P.M., G. F.S. and K.B.-d.-S., received scholarship from FAPESP, grant numbers 2016/12855-9; 2016/21259-0; 2018/13866-0; 2017/02402-0, 2016/07371-2; 2017/11828-0; 2017/26908-0, 2017/22062-9, 2018/13645-3, 2020/02159-0 and 2020/02448-2, respectively. National Council for Scientific and Technological Development (CNPq) supported D.A.T.-T. and M.C.M., grant numbers 141844/2019-1 and 421724/2017-0. Fundo de Apoio ao Ensino, Pesquisa e Extensão (FAEPEX) supported M.R.A., grant number 208/17. J.L.P.-M. was supported by CNPq grant number 305628/2020-8.

Disclaimer.

The funders had no role in study design, data collection and analysis, decision to publish, or preparation of the manuscript.

Appendix A. Supplementary data

Supplementary data to this article can be found online at https://doi.org/10.1016/j.bbi.2021.08.008.

References

Alciato, F., et al., TNF-alpha, IL-6, and IL-1 expression is inhibited by GAS6 in monocytes/macrophages. J Leukoc Biol, 2010. 87(5): p. 869-75. Available from: 10.1189/jlb.0909610.

Azamor, T., et al., 2020. Congenital Zika Syndrome is associated with interferon alfa receptor 1. BioRxiv preprint. https://doi.org/10.1101/715862. Available from: doi.org/10.1101/715862.

Bhattacharyya, S., et al., Enveloped viruses disable innate immune responses in dendritic cells by direct activation of TAM receptors. Cell Host Microbe, 2013. 14(2): p. 136-47. Available from: 10.1016/j.chom.2013.07.005.

Bowen, J.R., et al., Zika Virus Antagonizes Type I Interferon Responses during Infection of Human Dendritic Cells. PLoS Pathog, 2017. 13(2): p. e1006164. Available from: 10.1371/journal.ppat.1006164.

Cao-Lormeau, V.M., et al., Guillain-Barré Syndrome outbreak associated with Zika virus infection in French Polynesia: a case-control study. Lancet, 2016. 387(10027): p. 1531-1539. Available from: 10.1016/S0140-6736(16)00562-6.

Chaix, J., et al., Cutting edge: Priming of NK cells by IL-18. J Immunol, 2008. 181(3): p. 1627-31. Available from: 10.4049/jimmunol.181.3.1627.

Chen, J., Yang, Y., Yang, Y. et al . AXL promotes Zika virus infection in astrocytes by antagonizing type I interferon signalling. Nat Microbiol, 2018(3): p. 302–309. Available from: 10.1038/s41564-017-0092-4.

Cugola, F.R., et al., The Brazilian Zika virus strain causes birth defects in experimental models. Nature, 2016. 534(7606): p. 267-71. Available from: 10.1038/nature18296.

Dang, J., et al., Zika Virus Depletes Neural Progenitors in Human Cerebral Organoids through Activation of the Innate Immune Receptor TLR3. Cell Stem Cell, 2016. 19 (2): p. 258-265. Available from: 10.1016/j.stem.2016.04.014.

Davra, V., et al., Ligand Activation of TAM Family Receptors-Implications for Tumor Biology and Therapeutic Response. Cancers (Basel), 2016. 8(12). Available from: 10.3390/cancers8120107.

de Araújo, T.V.B., et al., Association between microcephaly, Zika virus infection, and other risk factors in Brazil: final report of a case-control study. Lancet Infect Dis, 2018. 18(3): p. 328-336. Available from: 10.1016/S1473-3099(17)30727-2.

Duffy, M.R., et al., Zika virus outbreak on Yap Island, Federated States of Micronesia. N Engl J Med, 2009. 360(24): p. 2536-4Available from: 10.1056/NEJMoa0805715.

Figueiredo, C.P., et al., Zika virus replicates in adult human brain tissue and impairs synapses and memory in mice. Nat Commun, 2019. 10(1): p. 3890. Available from: 10.1038/s41467-019-11866-7.

Foo, S.S., et al., Asian Zika virus strains target CD14(+) blood monocytes and induce M2-skewed immunosuppression during pregnancy. Nat Microbiol, 2017. 2(11): p. 1558-1570. Available from: 10.1038/s41564-017-0016-3.

França, G.V., et al., Congenital Zika virus syndrome in Brazil: a case series of the first 1501 livebirths with complete investigation. Lancet, 2016. 388(10047): p. 891-7. Available from: 10.1016/S0140-6736(16)30902-3.

Gong, S., et al., Plasma sMer, sAxl and GAS6 levels correlate with disease activity and severity in lupus nephritis. Eur J Clin Invest, 2019. 49(3): p. e13064. Available from: 10.1111/eci.13064.

Hamel, R., et al., Biology of Zika Virus Infection in Human Skin Cells. J Virol, 2015. 89 (17): p. 8880-96. Available from: 10.1128/JVI.00354-15.

Hastings, A.K., et al., TAM Receptors Are Not Required for Zika Virus Infection in Mice. Cell Rep, 2017. 19(3): p. 558-568. Available from: 10.1016/j.celrep.2017.03.058.

Hastings, A.K., et al., Loss of the TAM Receptor Axl Ameliorates Severe Zika Virus Pathogenesis and Reduces Apoptosis in Microglia. iScience, 2019. 13: p. 339-350. Available from: 10.1016/j.isci.2019.03.003.

Ioos, S., et al., Current Zika virus epidemiology and recent epidemics. Med Mal Infect, 2014. 44(7): p. 302-7. Available from: 10.1016/j.medmal.2014.04.008.

Jiang, L., et al., Plasma level of growth arrest-specific 6 (GAS6) protein and genetic variations in the GAS6 gene in patients with acute coronary syndrome. Am J Clin Pathol, 2009. 131(5): p. 738-43. Available from: 10.1309/AJCP3CX3AUVRBHCF.

Judice, C.C., et al., Efficient detection of Zika virus RNA in patients' blood from the 2016 outbreak in Campinas, Brazil. Sci Rep, 2018. 8(1): p. 4012. Available from: 10.1038/s41598-018-22159-2.

Kalita, J., U.K. Misra, and M. Das, Neurophysiological criteria in the diagnosis of different clinical types of Guillain-Barre syndrome. J. Neurol. Neurosurg. Psychiatry, 2008. 79(3): p. 289-93. Available from: 10.1136/jnnp.2007.118000.

Kam, Y.W., et al., Specific Biomarkers Associated With Neurological Complications and Congenital Central Nervous System Abnormalities From Zika Virus-Infected Patients in Brazil. J. Infect. Dis., 2017. 216(2): p. 172-181. Available from: 10.1093/infdis/jix261.

Kirane, A., et al., Warfarin Blocks Gas6-Mediated Axl Activation Required for Pancreatic Cancer Epithelial Plasticity and Metastasis. Cancer Res, 2015. 75(18): p. 3699-705. Available from: 10.1158/0008-5472.CAN-14-2887-T.

Laureti, M., et al., Flavivirus Receptors: Diversity, Identity, and Cell Entry. Front Immunol, 2018. 9: p. 2180. Available from: 10.1016/j.virol.2014.09.009.

Lemke, G. and C.V. Rothlin, Immunobiology of the TAM receptors. Nat Rev Immunol, 2008. 8(5): p. 327-36. Available from: 10.1038/nri2303.

Liu, S., et al., AXL-Mediated Productive Infection of Human Endothelial Cells by Zika Virus. Circ Res, 2016. 119(11): p. 1183-1189. Available from: 10.1161/CIRCRESAHA.116.309866.

Lupton, K., Zika virus disease: a public health emergency of international concern. Br J Nurs, 2016. 25(4): p. 198, 200-Available from: 10.12968/bjon.2016.25.4.198.

Ma, W., et al., Zika Virus Causes Testis Damage and Leads to Male Infertility in Mice. Cell, 2017. 168(3): p. 542. Available from: 10.1016/j.cell.2016.11.016.

Meertens, L., et al., The TIM and TAM families of phosphatidylserine receptors mediate dengue virus entry. Cell Host Microbe, 2012. 12(4): p. 544-57. Available from: 10.1016/j.chom.2012.08.009.

Meertens, L., et al., Axl Mediates ZIKA Virus Entry in Human Glial Cells and Modulates Innate Immune Responses. Cell Rep, 2017. 18(2): p. 324-333. Available from: 10.1016/j.celrep.2016.12.045.

Michlmayr, D., et al., CD14(+)CD16(+) monocytes are the main target of Zika virus infection in peripheral blood mononuclear cells in a paediatric study in Nicaragua. Nat Microbiol, 2017. 2(11): p. 1462-1470. Available from: 10.1038/s41564-017-0035-0.

Miner, J.J. and M.S. Diamond, Zika Virus Pathogenesis and Tissue Tropism. Cell Host Microbe, 2017. 21(2): p. 134-142. Available from: 10.1016/j.chom.2017.01.004.

Miner, J.J., et al., The TAM receptor Mertk protects against neuroinvasive viral infection by maintaining blood-brain barrier integrity. Nat Med, 2015. 21(12): p. 1464-72. Available from: 10.1038/nm.3974.

Miner, J.J., et al., Zika Virus Infection in Mice Causes Panuveitis with Shedding of Virus in Tears. Cell Rep, 2016. 16(12): p. 3208-3218. Available from: 10.1016/j.celrep.2016.08.079.

Mlakar, J., et al., Zika Virus Associated with Microcephaly. N Engl J Med, 2016. 374(10): p. 951-8. Available from: 10.1056/NEJMoa1600651.

Moller-Tank, S., Maury, W. Phosphatidylserine receptors: enhancers of enveloped virus entry and infection. Virology, 2014. 468-470: p. 565-580. Available from: 10.1016/j.virol.2014.09.009.

Morizono, K., et al., The soluble serum protein Gas6 bridges virion envelope phosphatidylserine to the TAM receptor tyrosine kinase Axl to mediate viral entry. Cell Host Microbe, 2011. 9(4): p. 286-98. Available from: 10.1016/j.chom.2011.03.012.

Muñoz, X., et al., 2007. Association of specific haplotypes of GAS6 gene with stroke. Thromb Haemost 98 (2), 406–412.

Muñoz, X., et al., Human vitamin K-dependent GAS6: gene structure, allelic variation, and association with stroke. Hum Mutat, 2004. 23(5): p. 506-12. Available from: 10.1002/humu.20025.

Nakano, T., et al., Requirement of gamma-carboxyglutamic acid residues for the biological activity of Gas6: contribution of endogenous Gas6 to the proliferation of vascular smooth muscle cells. Biochem J, 1997. 323 (Pt 2): p. 387-92. Available from: 10.1042/bj3230387.

Nikolskaia, O.V., et al., Blood-brain barrier traversal by African trypanosomes requires calcium signaling induced by parasite cysteine protease. J Clin Invest, 2006. 116 (10): p. 2739-47. Available from: 10.1172/JCI27798.

Nobrega, G.M., et al., TAM and TIM receptors mRNA expression in Zika virus infected placentas. Placenta, 2020. 101: p.204–207. Available from: 10.1016/j.placenta.2020.09.062.

Oliveira, L.G. and J.P.S. Peron, Viral receptors for flaviviruses: Not only gatekeepers. J Leukoc Biol, 2019. 106(3): p. 695-701. Available from: 10.1002/JLB.MR1118-460R.

Ozakpinar, O.B., et al., Association between the growth arrest-specific 6 (Gas6) gene polymorphism c.834 + 7G>A and preeclampsia. J Matern Fetal Neonatal Med, 2016. 29(7): p. 1149-53. Available from: 10.3109/14767058.2015.1038516.

Papa, M.P., et al., Zika Virus Infects, Activates, and Crosses Brain Microvascular Endothelial Cells, without Barrier Disruption. Front Microbiol, 2017. 8: p. 2557. Available from: 10.3389/fmicb.2017.02557.

Peng, S., et al., Plasma levels of TAM receptors and ligands in severe preeclampsia. Pregnancy Hypertens, 2018. 13: p. 116-120. Available from: 10.1016/j.preghy.2018.05.012.

Perera-Lecoin, M., et al., Flavivirus entry receptors: an update. Viruses, 2013. 6(1): p. 69-88. Available from: 10.3390/v6010069.

Proenca-Modena, J.L., et al., Zika virus: lessons learned in Brazil. Microbes Infect, 2018. 20(11-12): p. 661-669. Available from: 10.1016/j.micinf.2018.02.008.

Rasmussen, S.A., et al., Zika Virus and Birth Defects–Reviewing the Evidence for Causality. N Engl J Med, 2016. 374(20): p. 1981-7. Available from: 10.1056/NEJMsr1604338.

Richard, A.S., et al., AXL-dependent infection of human fetal endothelial cells distinguishes Zika virus from other pathogenic flaviviruses. Proc Natl Acad Sci U S A, 2017. 114(8): p. 2024-2029. Available from: 10.1073/pnas.1620558114.

Rothlin, C.V., et al., TAM receptors are pleiotropic inhibitors of the innate immune response. Cell, 2007. 131(6): p. 1124-36. Available from: 10.1016/j.cell.2007.10.034.

Russo, F.B., Jungmann, P., Beltrão-Braga, P.C.B., Zika infection and the development of neurological defects. Cell Microbiol,, 2017. **19**(6). Available from. https://doi.org/10.1111/cmi.12744.

Smirne, C., et al., Gas6/TAM Signaling Components as Novel Biomarkers of Liver Fibrosis. Dis Markers, 2019. 2019: p. 2304931. Available from: 10.1155/2019/2304931.

Soares de Oliveira-Szejnfeld, P., et al., Congenital Brain Abnormalities and Zika Virus: What the Radiologist Can Expect to See Prenatally and Postnatally. Radiology, 2016. 281(1): p. 203-18. Available from: 10.1148/radiol.2016161584.

Souza, I.N.O., et al., Late Neurological Consequences of Zika Virus Infection: Risk Factors and Pharmaceutical Approaches. Pharmaceuticals (Basel), 2019. 12(2). Available from: 10.3390/ph12020060.

Souza, W.M., et al., Viral diversity of Rhipicephalus microplus parasitizing cattle in southern Brazil. Sci Rep, 2018. 8(1): p. 16315. Available from: 10.1038/s41598-018-34630-1.

Sun, X., et al., Transcriptional Changes during Naturally Acquired Zika Virus Infection Render Dendritic Cells Highly Conducive to Viral Replication. Cell Rep, 2017. 21 (12): p. 3471-3482. Available from: 10.1016/j.celrep.2017.11.087.

Tjwa, M., et al., Gas6 promotes inflammation by enhancing interactions between endothelial cells, platelets, and leukocytes. Blood, 2008. 111(8): p. 4096-105. Available from: 10.1182/blood-2007-05-089565.

van den Pol, A.N., et al., Zika Virus Targeting in the Developing Brain. J Neurosci, 2017. 37(8): p. 2161-2175. Available from: 10.1523/JNEUROSCI.3124-16.2017.

van der Meer, J.H., T. van der Poll, and C. van 't Veer, TAM receptors, Gas6, and protein S: roles in inflammation and hemostasis. Blood, 2014. 123(16): p. 2460-9. Available from: 10.1182/blood-2013-09-528752.

Venkatesan, A., et al., Case definitions, diagnostic algorithms, and priorities in encephalitis: consensus statement of the international encephalitis consortium. Clin Infect Dis, 2013. 57(8): p. 1114-28. Available from: 10.1093/cid/cit458.

Ventura, C.V., et al., Ophthalmological findings in infants with microcephaly and presumable intra-uterus Zika virus infection. Arq Bras Oftalmol, 20179(1): p. 1-3. Available from: 10.5935/0004-2749.20160002.

Waggoner, J.J., et al., 2016. Viremia and Clinical Presentation in Nicaraguan Patients Infected With Zika Virus, Chikungunya Virus, and Dengue Virus. Clin. Infect. Dis. 63 (12), 1584–1590. Available from:10.1093/cid/ciw589.

Wu, K.Y., et al., Vertical transmission of Zika virus targeting the radial glial cells affects cortex development of offspring mice. Cell Res, 2016. 26(6): p. 645-54. Available from: 10.1038/cr.2016.58.

Yockey, L.J., Type, I., interferons instigate fetal demise after Zika virus infection. Sci Immunol,, et al., 2018. **3**(19). Available from. https://doi.org/10.1126/sciimmunol.aao1680.

Yuan, L., et al., A single mutation in the prM protein of Zika virus contributes to fetal microcephaly. Science, 2017. 358(6365): p. 933-936. Available from: 10.1126/science.aam7120.

Zhao, G.J., et al., Growth Arrest-Specific 6 Enhances the Suppressive Function of CD4. Mediators Inflamm, 2017. 2017: p. 6848430. Available from: 10.1155/2017/6848430.